OPEN ACCESS
International Journal of Bifurcation and Chaos, Vol. 34, No. 1 (2024) 2450001 (26 pages)

DOI: 10.1142/S0218127424500019

New Class of Discrete-Time Memristor Circuits: First Integrals, Coexisting Attractors and Bifurcations Without Parameters

Mauro Di Marco*, Mauro Forti† and Luca Pancioni‡
Department of Information Engineering and Mathematics, University of Siena, via Roma 56, 53100 Siena, Italy
**mauro.dimarco@unisi.it*
†*forti@diism.unisi.it*
‡*pancioni@diism.unisi.it*

Alberto Tesi
Department of Information Engineering, University of Florence, via Santa Marta 3, 50139 Firenze, Italy
alberto.tesi@unifi.it

Received November 3, 2023; Accepted November 14, 2023

The use of ideal memristors in a continuous-time (CT) nonlinear circuit is known to greatly enrich the dynamic behavior with respect to the memristorless counterpart, which is a crucial property for applications in future analog electronic circuits. This can be explained via the flux–charge analysis method (FCAM), according to which CT circuits with ideal memristors have for structural reasons *first integrals* (*or invariants of motion*, *or conserved quantities*) and their state space can be foliated in infinitely many invariant manifolds where they can display different dynamics. The paper introduces a new discretization scheme for the memristor which, differently from those adopted in the literature, guarantees that *the first integrals of the CT memristor circuits are preserved exactly in the discretization*, and that this is true *for any step size*. This new scheme makes it possible to extend FCAM to discrete-time (DT) memristor circuits and rigorously show the existence of invariant manifolds and infinitely many coexisting attractors (extreme multistability). Moreover, the paper addresses standard bifurcations varying the discretization step size and also bifurcations without parameters, i.e. bifurcations due to varying the initial conditions for fixed step size and circuit parameters. The method is illustrated by analyzing the dynamics and flip bifurcations with and without parameters in a DT memristor–capacitor circuit and the Poincaré–Andronov–Hopf bifurcation in a DT Murali–Lakshmanan–Chua circuit with a memristor. Simulations are also provided to illustrate bifurcations in a higher-order DT memristor Chua's circuit. The results in the paper show that DT memristor circuits obtained with the proposed discretization scheme are able to display even richer dynamics and bifurcations than their CT counterparts, due to the coexistence of infinitely many attractors and

†Author for correspondence

the possibility to use the discretization step as a parameter without destroying the foliation in invariant manifolds.

Keywords: Bifurcation without parameters; discrete-time memristor circuit; first integral; flip bifurcation; flux-charge analysis method; invariant manifold; memristor; Poincaré–Andronov–Hopf bifurcation.

1. Introduction

The memristor was postulated in a seminal article by Chua [1971] as the fourth basic passive circuit element in addition to the resistor, capacitor and inductor. Due to the lack of physical devices for implementing a memristor, the memristor itself has been mainly of theoretic and academic interest for more than 30 years. Things changed drastically due to the discovery of memristive behavior in nanotechnology devices by Williams and his team [Strukov *et al.*, 2008]. Since then, the memristor has been the subject of an unprecedented research interest due to its enormous potential for implementing compact and power-efficient memories and its expected role in futuristic neuromorphic computers [Yang & Williams, 2013; Williams, 2017; Sebastian *et al.*, 2018; Huang *et al.*, 2021; James *et al.*, 2018; Sirakoulis *et al.*, 2022].

One relevant research branch concerns the use of memristors in the design of continuous-time (CT) dynamic analog circuits for signal processing. In fact, several papers in the literature have pointed out that, due to their memory and nonlinearity, memristors are able to greatly enrich the possible range of dynamic behaviors, which is crucial for the use of analog circuits in future electronics [Itoh & Chua, 2008; Ascoli *et al.*, 2022a, 2022b; Buscarino *et al.*, 2013; Kumar *et al.*, 2017; Liang *et al.*, 2020].

In recent years, a technique named flux–charge analysis method (FCAM) has been introduced to analyze CT circuits with ideal memristors in the flux–charge domain (FCD), rather than in the traditional voltage–current domain (VCD) [Corinto & Forti, 2016; Corinto *et al.*, 2021]. By means of FCAM, it has been shown that any circuit with ideal memristors admits for structural reasons first integrals and the state space can be foliated in infinitely many invariant manifolds where it displays different dynamics [Corinto & Forti, 2017]. This rigorously shows that memristor circuits can possess infinitely many different coexisting attractors, a peculiar dynamic property known in the literature as extreme multistability [Hens *et al.*, 2012; Bao *et al.*, 2016; Chang *et al.*, 2019]. When applied for instance to a memristor Chua's circuit (MCC), FCAM shows that there is coexistence of convergent, periodic and complex dynamics for a given set of MCC parameters. In Di Marco *et al.* [2022] and Escudero *et al.* [2023], it is shown that extreme multistability can be observed also in circuits with some real memristor devices.

The study of discrete-time (DT) models of memristors is rapidly gaining increasing interest and momentum in the literature due a number of fundamental reasons:

(a) Real memristor devices for laboratory experiments are nowadays still not always easily available, hence DT models permit to develop effective digital emulators to study the dynamics and evaluate the performance of CT memristor circuits [Itoh & Chua, 2014; Solan & Ochs, 2018]. DT emulators of memristors can be directly implemented in software on digital computers or other types of digital signal processors, as a reconfigurable hardware emulator on an FPGA (field-programmable gate array) or an ASIC (application-specific integrated circuit).
(b) In addition to approximating the dynamics of CT counterparts, discrete maps implemented by DT memristor circuits can be of interest in themselves as a source of complex dynamics for engineering applications. Along this line, several papers in the literature have been devoted to DT memristor circuits generating chaos or hyperchaos and exhibiting coexisting complex attractors, see e.g. Bao *et al.* [2021], Bao *et al.* [2022] and Li *et al.* [2020] and references therein. Industrial applications to generate chaotic sequences of numbers or chaotic signals in secure communications have been investigated in these papers as well.
(c) DT models of memristors can be effectively used for implementing on a digital hardware relevant paradigms such as DT cellular neural

networks and cellular automata [Di Marco *et al.*, 2023; Itoh & Chua, 2014].

Despite considerable works available so far in the literature, a rigorous analysis of how the properties of the dynamics of CT memristor circuits are affected by the discretization schemes is still lacking. This paper addresses this issue by introducing a new method to analyze a large class of DT memristor circuits, named $\mathcal{LM}$, containing ideal memristors, capacitors, inductors, resistors and possibly voltage and current sources. More precisely, the goal of this paper is threefold:

(1) The fact that a CT system has a first integral is known to be a fragile property, i.e. it is in general not preserved when discretizing the system, no matter how small the step size is. This notwithstanding, in the paper we introduce a *new ad-hoc discretization scheme* for the memristor which, differently from the schemes used in the literature, guarantees that the first integrals and the foliation in invariant manifolds of the state space are *preserved exactly in the discretization*, *and that this property holds for any step size*.
(2) The paper extends FCAM in order to analyze in the FCD the DT memristor circuits thus obtained. The new method is named the discrete-time flux–charge analysis method, or DT-FCAM.
(3) The paper illustrates the application of DT-FCAM to rigorously show the existence of infinitely many coexisting attractors (extreme multistability) for some prototypical circuits in $\mathcal{LM}$, namely, a DT memristor–capacitor (MC) circuit, a DT Murali–Lakshmanan–Chua circuit with a memristor and a DT memristor Chua's circuit. More precisely, the paper studies two types of bifurcations: First, standard bifurcations with respect to the step size, using the property that the existence of invariant manifolds and their structure is independent of the step size; second, it addresses bifurcations without parameters for a fixed step size.

The results in the paper show that DT memristor circuits in $\mathcal{LM}$ obtained with the proposed scheme are able to display even richer dynamics and bifurcations than the original CT circuits. This property is due to the possibility for varying the step size without altering the structure of invariant manifolds and the coexistence of infinitely many different attractors for each fixed step size.

2. Basic Example

For illustrative purposes, we find it useful to discuss the basic idea in this paper by means of the simplest memristor circuit. More precisely, consider the CT memristor–capacitor (MC) circuit in Fig. 1, given by a linear capacitor $i_C = C\dot{v}_C$, where the dot denotes the time derivative, and a flux-controlled memristor $q_M = \hat{q}(\varphi_M)$, where $\varphi_M(t) = \int_{-\infty}^{t} v_M(t)dt$ and $q_M(t) = \int_{-\infty}^{t} i_M(t)$ are the memristor flux and charge, respectively. The MC circuit satisfies the second-order ordinary differential equation (ODE) in the state variables v_C, φ_M,

$$\begin{cases} \dot{v}_C = -\dfrac{1}{C}\hat{q}'(\varphi_M)v_C, \\ \dot{\varphi}_M = v_C, \end{cases} \tag{1}$$

for $t \geq t_0$, where t_0 is the initial instant. By $\hat{q}'$, we denote the derivative of $\hat{q}$ with respect to its argument.

Consider the function of the state variables

$$w(v_C, \varphi_M) = Cv_C + \hat{q}(\varphi_M).$$

We have

$$\dot{w}(v_C(t), \varphi_M(t)) = C\dot{v}_C(t) + \hat{q}'(\varphi_M(t))\dot{\varphi}_M(t) = 0,$$

i.e. w is constant along the solutions of (1). In mathematical terms, w is said to be a *first integral* (*or invariant of motion*, *or conserved quantity*) of the MC circuit.

The existence of a first integral is of importance, since it severely constrains the dynamics of the MC circuit, which is bound to evolve on invariant manifolds; moreover, on each invariant manifold the dynamics itself turns out to be of lower order (i.e. first-order) [Corinto & Forti, 2016]. The

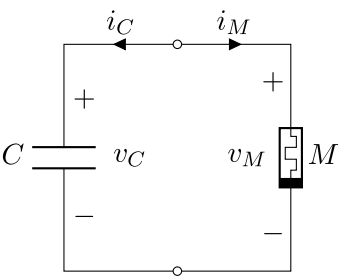

Fig. 1. Continuous-time MC circuit.

existence of a first integral and the foliation of the state space in invariant manifolds permit to explain rigorously the coexistence of an infinite number of attractors for the MC circuit, a phenomenon also known as extreme multistability. Moreover, they are at the basis of the so-called bifurcations without parameters.

Now, suppose we want to discretize the ODE (1). Given a scalar function $x(t)$, $t \geq t_0$, we consider its samplings $x_k \doteq x(t_k) = x(t_0 + kh)$, $k = 0, 1, 2, \ldots$, where $h > 0$ is the step size (or sampling interval). According to the forward Euler rule, $\dot{x}(t_k)$ can be approximated by the difference quotient

$$\begin{aligned}\dot{x}(t_k) &= \frac{x(t_{k+1}) - x(t_k)}{h} \\ &= \frac{x(t_0 + (k+1)h) - x(t_0 + kh)}{h} \\ &= \frac{x_{k+1} - x_k}{h}.\end{aligned}$$

Next, we consider two different discretization schemes for (1).

Discretization Scheme 1. A first possibility is to consider the scheme

$$\begin{cases} v_{C,k+1} = v_{C,k} - h\hat{q}'(\varphi_{M,k})v_{C,k}, \\ \varphi_{M,k+1} = \varphi_{M,k} + hv_{C,k}, \end{cases} \tag{2}$$

where we used the forward Euler rule to approximate $\dot{v}_C(t_k)$ and $\dot{\varphi}_M(t_k)$. This is a second-order map in the state variables $v_{C,k}$, $\varphi_{M,k}$ defining a DT MC circuit.

It can be checked that w *is no longer a first integral* for the map (2) no matter how small the step size h is. In fact, we have

$$\begin{aligned}\Delta w_k &\doteq w(v_{C,k+1}, \varphi_{M,k+1}) - w(v_{C,k}, \varphi_{M,k}) \\ &= -h\hat{q}'(\varphi_{M,k})v_{C,k} + \hat{q}(\varphi_{M,k} + hv_k) \\ &\quad - \hat{q}(\varphi_{M,k}).\end{aligned}$$

Since in the general case

$$\hat{q}'(\varphi_{M,k}) \neq \frac{\hat{q}(\varphi_{M,k} + hv_k) - \hat{q}(\varphi_{M,k})}{hv_{C,k}},$$

it follows that $\Delta w_k \neq 0$, i.e. w is not constant along the solutions of (2).

It is worth noting that this is the *typical discretization scheme* used in the literature to study the DT memristor circuits, see e.g. Bao *et al.* [2021], Bao *et al.* [2022] and Li *et al.* [2020] and references therein.

Discretization Scheme 2. The new discretization proposed in this paper is as follows. Recall that $i_M = \dot{q}_M$. By the forward Euler rule, we have $i_{M,k} = (q_{M,k+1} - q_{M,k})/h = (\hat{q}(\varphi_{M,k+1}) - \hat{q}(\varphi_{M,k}))/h$. Therefore, we obtain the scheme

$$\begin{cases} v_{C,k+1} = v_{C,k} - \dfrac{1}{C}(\hat{q}(\varphi_{M,k} + hv_{C,k}) - \hat{q}(\varphi_{M,k})), \\ \varphi_{M,k+1} = \varphi_{M,k} + hv_{C,k}. \end{cases} \tag{3}$$

This is again a second-order map in the state variables $v_{C,k}, \varphi_{M,k}$.

Now, it can be checked that

$$\begin{aligned}w(v_{C,k+1}, \varphi_{M,k+1}) &= Cv_{C,k+1} + \hat{q}(\varphi_{M,k+1}) \\ &= w(v_{C,k}, \varphi_{M,k}) \\ &= Cv_{C,k} + \hat{q}(\varphi_{M,k}),\end{aligned}$$

hence $\Delta w_k = 0$. Therefore, it can be concluded that, using the second discretization scheme, the first integral w *is preserved exactly in the discretization of MC for any step size* h.

The possibility to use a discretization scheme that exactly preserves the first integral is crucial. In Sec. 4, we will continue the analysis of map (3) showing that, due to the existence of a first integral, the state space can be foliated in invariant manifolds where the map is of lower order (first-order), and giving a rigorous proof of the coexistence of an infinite number of attractors and the existence of bifurcations without parameters for the DT MC circuit, in analogy to what happens in the CT case. To this end, we will find it useful to analyze the DT MC circuit not only in the traditional VCD, but also in the FCD.

3. Discrete-Time Flux–Charge Analysis Method

In this section, we extend the ideas in Sec. 2 by developing a general method to discretize and analyze DT memristor circuits. Let us consider a class of CT memristor circuits named $\mathcal{LM}$ containing two-terminal elements such as ideal resistors, capacitors and inductors, ideal flux-controlled or charge-controlled memristors and possibly independent voltage or current sources. Corinto and Forti [2016, 2017] (see also Corinto *et al.* [2021])

developed a method to effectively analyze such class of circuits in the FCD, rather than in the traditional VCD, named the flux–charge analysis method. FCAM permits to show that any circuit in $\mathcal{LM}$ possesses for structural reasons one or more first integrals, so that the state space can be foliated in invariant manifolds where there is a reduced-order dynamics. In this section, we address two main issues: (a) to introduce a new discretization scheme for CT circuits in $\mathcal{LM}$; and (b) to develop a method to effectively analyze the DT memristor circuits thus obtained in the FCD, based on writing the Kirchhoff laws and constitutive relations (CRs) of the DT circuit elements in the FCD. We will name such method the DT-FCAM. In Sec. 4, we will apply DT-FCAM to some basic DT memristor circuits in $\mathcal{LM}$, namely, an MC circuit, a Murali–Lakshmanan–Chua circuit with a memristor and a memristor Chua's circuit, and we will show that the newly introduced discretization scheme guarantees that the first integrals of CT memristor circuits are preserved exactly in the discretization for any step size. This will enable us to prove for these circuits the coexistence of infinite attractors (extreme multistability) and to study bifurcations without parameters.

3.1. *Electric quantities and Kirchhoff laws*

For each circuit element in $\mathcal{LM}$, in addition to the voltage v and current i, we consider the flux $\varphi(t) = \int_{-\infty}^{t} v(t)dt$ and charge $q(t) = \int_{-\infty}^{t} i(t)dt$. Moreover, given an initial instant t_0, for $t \geq t_0$, we define the incremental flux $\varphi^0(t) = \varphi(t) - \varphi(t_0) = \int_{t_0}^{t} v(t)dt$ and incremental charge $q^0(t) = q(t) - q(t_0) = \int_{t_0}^{t} i(t)dt$ [Corinto & Forti, 2016]. We have

$$v(t) = \frac{d\varphi(t)}{dt} = \frac{d\varphi^0(t)}{dt}, \quad i(t) = \frac{dq(t)}{dt} = \frac{dq^0(t)}{dt}.$$

Kirchhoff voltage law (KVL) can be expressed as

$$\sum_j v_j(t) = 0$$

for the voltages of the elements forming a loop, while Kirchhoff current law (KCL) can be expressed as

$$\sum_j i_j(t) = 0$$

for the currents of elements connected to a node. By integrating KVL and KCL between t_0 and $t \geq t_0$, we obtain the Kirchhoff (incremental) flux Law (KφL)

$$\sum_j \varphi_j^0(t) = 0$$

and the Kirchhoff (incremental) charge law (KqL)

$$\sum_j q_j^0(t) = 0.$$

It is worth to stress that, as it is discussed in detail in Corinto and Forti [2016], it is not convenient to use analogous forms of these laws involving the flux or charge.

Consider the sampling instants $t_k = t_0 + kh$, $k = 0, 1, 2, \ldots$, where the step size $h > 0$, and the discretized electric quantities $v_k = v(t_k)$, $i_k = i(t_k)$, $\varphi_k = \varphi(t_k)$, $q_k = q(t_k)$, $\varphi_k^0 = \varphi^0(t_k)$ and $q_k^0 = q^0(t_k)$. By the forward Euler rule, we obtain

$$v_k = \frac{\varphi_{k+1} - \varphi_k}{h} = \frac{\varphi_{k+1}^0 - \varphi_k^0}{h},$$

$$i_k = \frac{q_{k+1} - q_k}{h} = \frac{q_{k+1}^0 - q_k^0}{h}.$$

Moreover,

$$\dot{v}_k = \dot{v}(t_k) = \frac{v_{k+1} - v_k}{h},$$

$$\dot{i}_k = \dot{i}(t_k) = \frac{i_{k+1} - i_k}{h}.$$

Via discretization, the KVL reads as

$$\sum_j v_{j,k} = 0,$$

while the KCL is given by

$$\sum_j i_{j,k} = 0.$$

Moreover, KφL becomes

$$\sum_j \varphi_{j,k}^0 = 0,$$

while KqL can be expressed as

$$\sum_j q_{j,k}^0 = 0.$$

3.2. *Constitutive relations of circuit elements*

In the previous subsection, we have introduced the DT versions of Kirchhoff laws in terms of voltages and currents (VCD), and the corresponding ones involving incremental fluxes and charges (FCD). Here, we address the problem of writing the DT versions of CRs of circuit elements both in the VCD and FCD. To be more specific, by a CR in the VCD we mean a relation between v_k and i_k possibly involving other internal state variables. Similarly, by a CR in the FCD we mean a relation between φ_k^0 and q_k^0 possibly involving other internal state variables.

3.2.1. *Capacitor*

Consider a linear capacitor with CR $q_C = Cv_C$. We have (VCD)

$$i_C = C\dot{v}_C.$$

The CR in terms of incremental flux and charge (FCD) is given by the first-order ODE [Corinto & Forti, 2016]

$$q_C^0(t) = C\dot{\varphi}_C^0(t) - Cv_C(t_0).$$

Let us now discretize the capacitor. Applying the forward Euler rule, we obtain the first-order map (VCD)

$$i_{C,k} = C\frac{v_{C,k+1} - v_{C,k}}{h}. \tag{4}$$

Moreover, the CR in terms of incremental flux and charge (FCD) is given by the first-order map

$$q_{C,k}^0 = C\frac{\varphi_{C,k+1}^0 - \varphi_{C,k}^0}{h} - Cv_C(t_0). \tag{5}$$

3.2.2. *Inductor*

Consider a linear inductor with CR $\varphi_L = Li_L$. We have (VCD)

$$v_L = L\dot{i}_L.$$

The CR in terms of incremental flux and charge (FCD) is given by the first-order ODE [Corinto & Forti, 2016]

$$\varphi_L^0(t) = L\dot{q}_L^0(t) - Li_L(t_0).$$

Let us now discretize the inductor. Applying the forward Euler rule, we obtain the first-order map (VCD)

$$v_{L,k} = L\frac{i_{L,k+1} - i_{L,k}}{h}. \tag{6}$$

Moreover, the CR in terms of incremental flux and charge (FCD) is given by the first-order map

$$\varphi_{L,k}^0 = L\frac{q_{L,k+1}^0 - q_{L,k}^0}{h} - Li_L(t_0). \tag{7}$$

3.2.3. *Flux-controlled memristor*

Consider a flux-controlled memristor whose defining CR is $q_M = \hat{q}(\varphi_M)$. By differentiating in time, the CR in the VCD is given by

$$\begin{cases} i_M = \hat{q}'(\varphi_M)v_M, \\ \dot{\varphi}_M = v_M. \end{cases} \tag{8}$$

In the FCD, the CR in terms of the incremental flux and charge is the algebraic relation [Corinto & Forti, 2016]

$$q_M^0(t) = \hat{q}(\varphi_M^0(t) + \varphi_M(t_0)) - \hat{q}(\varphi_M(t_0)).$$

Let us now discretize the memristor. Analogous to Sec. 2, we consider two different discretization schemes.

Discretization Scheme 1. In the VCD, the typical discretization scheme of (8) considered in the literature is [Bao *et al.*, 2021; Bao *et al.*, 2022; Li *et al.*, 2020]

$$\begin{cases} i_{M,k} = \hat{q}'(\varphi_{M,k})v_{M,k}, \\ \varphi_{M,k+1} = \varphi_{M,k} + hv_{M,k}, \end{cases} \tag{9}$$

where the forward Euler rule is used in (8) to approximate $\dot{\varphi}_M = v_M$.

Discretization Scheme 2. In this paper, we introduce a new discretization scheme of (8) in the VCD as follows. By applying the forward Euler rule to $i_M = \dot{q}_M$, we have $i_{M,k} = (q_{M,k+1} - q_{M,k})/h = (\hat{q}(\varphi_{M,k+1}) - \hat{q}(\varphi_{M,k}))/h$. Therefore, we obtain the scheme

$$\begin{cases} i_{M,k} = \dfrac{\hat{q}(\varphi_{M,k+1}) - \hat{q}(\varphi_{M,k})}{h}, \\ \varphi_{M,k+1} = \varphi_{M,k} + hv_{M,k}. \end{cases} \tag{10}$$

It is worth to stress that on the basis of (10), $v_{M,k} = 0$ implies $i_{M,k} = 0$, hence the pinched

hysteresis property in response to a sinusoidal signal is preserved exactly in the discretization. From now on, unless stated otherwise, we always use the discretization scheme (10) for the memristor.

Finally, in the FCD we simply obtain the algebraic map

$$q^0_{M,k} = \hat{q}(\varphi^0_{M,k} + \varphi_M(t_0)) - \hat{q}(\varphi_M(t_0)). \quad (11)$$

3.2.4. *Charge-controlled memristor*

Consider a charge-controlled memristor whose defining CR is $\varphi_M = \hat{\varphi}(q_M)$. By differentiating in time, the CR in the VCD is given by

$$\begin{cases} v_M = \hat{\varphi}'(q_M) i_M, \\ \dot{q}_M = i_M. \end{cases} \quad (12)$$

In the FCD, the CR in terms of the incremental flux and charge is the algebraic relation [Corinto & Forti, 2016]

$$\varphi^0_M(t) = \hat{\varphi}(q^0_M(t) + q_M(t_0)) - \hat{\varphi}(q_M(t_0)).$$

Let us now discretize the memristor. We consider two different discretization schemes.

Discretization Scheme 1. In the VCD, the typical discretization scheme of (12) considered in the literature is

$$\begin{cases} v_{M,k} = \hat{\varphi}'(q_{M,k}) i_{M,k}, \\ q_{M,k+1} = q_{M,k} + h i_{M,k}, \end{cases} \quad (13)$$

where the forward Euler rule is used in (12) to approximate $\dot{q}_M = i_M$.

Discretization Scheme 2. In this paper, we introduce a new discretization scheme of (12) in the VCD as follows. By applying the forward Euler rule to $v_M = \dot{\varphi}_M$, we have $v_{M,k} = (\varphi_{M,k+1} - \varphi_{M,k})/h = (\hat{\varphi}(q_{M,k+1}) - \hat{\varphi}(q_{M,k}))/h$. Therefore, we obtain the scheme

$$\begin{cases} v_{M,k} = \dfrac{\hat{\varphi}(q_{M,k+1}) - \hat{\varphi}(q_{M,k})}{h}, \\ q_{M,k+1} = q_{M,k} + h i_{M,k}. \end{cases} \quad (14)$$

It is worth to stress that on the basis of (14), $i_{M,k} = 0$ implies $v_{M,k} = 0$, hence the pinched hysteresis property in response to a sinusoidal signal is preserved exactly in the discretization. From now on, unless stated otherwise, we always use the discretization scheme (14) for the memristor.

Finally, in the FCD we simply obtain the algebraic map

$$\varphi^0_{M,k} = \hat{\varphi}(q^0_{M,k} + q_M(t_0)) - \hat{\varphi}(q_M(t_0)). \quad (15)$$

3.2.5. *Resistor*

Consider a linear resistor $v_R = R i_R$ (VCD). In the FCD, we have $\varphi^0_R(t) = R q^0_R(t)$. By discretization, we obtain $v_{R,k} = R i_{R,k}$ in the VCD and $\varphi^0_{R,k} = R q^0_{R,k}$ in the FCD.

3.2.6. *Voltage and current source*

Consider an ideal voltage source $v(t) = \hat{v}(t)$, where $\hat{v}$ is a given function (VCD). In the FCD, we have $\varphi^0(t) = \int_{t_0}^t \hat{v}(\sigma) d\sigma$. By discretization, we obtain $v_k = \hat{v}_k$ in the VCD and $\varphi^0_k = \int_{t_0}^{t_0+kh} \hat{v}(\sigma) d\sigma$ in the FCD.

We proceed in an analogous way for an ideal current source $i(t) = \hat{i}(t)$, where $\hat{i}$ is a given function (VCD). In the FCD, we have $q^0(t) = \int_{t_0}^t \hat{i}(\sigma) d\sigma$. By discretization, we obtain $i_k = \hat{i}_k$ in the VCD and $q^0_k = \int_{t_0}^{t_0+kh} \hat{i}(\sigma) d\sigma$ in the FCD.

4. Analysis of MC Circuit via DT-FCAM

4.1. *Analysis in the VCD*

Let us analyze the DT MC circuit in the class $\mathcal{LM}$ shown in Fig. 2, with an ideal capacitor $C > 0$ and an ideal flux-controlled memristor $q_M = \hat{q}(\varphi_M)$, using DT-FCAM and the new discretization scheme introduced for the memristor. In the VCD, KCL reads as $i_{C,k} + i_{M,k} = 0$. Using the CR of C given by (4) and the second discretization scheme for M, i.e. the CR (10), we obtain

$$C \frac{v_{C,k+1} - v_{C,k}}{h} + \frac{\hat{q}(\varphi_{M,k+1}) - \hat{q}(\varphi_{M,k})}{h} = 0.$$

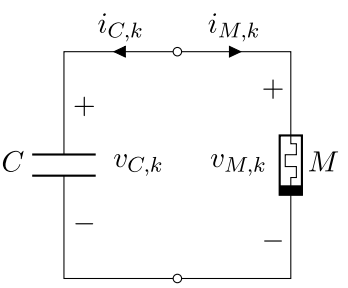

Fig. 2. Discrete-time MC circuit.

KVL yields $v_{C,k} = v_{M,k}$, hence

$$\varphi_{M,k+1} = \varphi_{M,k} + hv_{M,k} = \varphi_{M,k} + hv_{C,k}.$$

Therefore, we obtain in the VCD the second-order map in the state variables $v_{C,k}, \varphi_{M,k}$,

$$\begin{cases} v_{C,k+1} = v_{C,k} + \dfrac{1}{C}(-\hat{q}(\varphi_{M,k} + hv_{C,k}) + \hat{q}(\varphi_{M,k})), \\ \varphi_{M,k+1} = \varphi_{M,k} + hv_{C,k}, \end{cases} \tag{16}$$

which coincides with that found in Sec. 2. The initial conditions are $v_{C,0} = v_C(t_0)$ and $\varphi_{M,0} = \varphi_M(t_0)$.

4.2. *First integral and invariant manifolds*

Consider the function of the state variables

$$w(v_C, \varphi_M) = Cv_C + \hat{q}(\varphi_M).$$

We have

$$w(v_{C,k+1}, \varphi_{M,k+1}) = w(v_{C,k}, \varphi_{M,k})$$

along the solutions of (16). Hence, as it was already noticed in Sec. 2, w is a first integral for the DT MC circuit and it coincides with that of the CT MC circuit. Note that this holds for any step size h.

Let us introduce the subsets of the state space

$$\mathcal{M}(Q_0) = \{(v_C, \varphi_M) \in \mathbb{R}^2 : w(v_C, \varphi_M) = Cv_C + \hat{q}(\varphi_M) = Q_0\},$$

where $Q_0 \in \mathbb{R}$. Each set is a one-dimensional *invariant manifold* for the dynamics of (16) and it is uniquely defined by the *manifold index* $Q_0 = Cv_{C,0} + \hat{q}(\varphi_{M,0})$ depending upon the initial conditions for the state variables in the VCD.

It is worth to stress that the first integral w and the invariant manifolds $\mathcal{M}(Q_0)$ are independent of the step size h.

4.3. *Analysis in the FCD*

Let us now analyze the DT MC circuit in Fig. 3 in the FCD in order to determine the dynamics on each invariant manifold. We have from KqL that $q^0_{C,k} + q^0_{M,k} = 0$. Using the CR of C given by (5) and the CR of M in (11), we have

$$C\frac{\varphi^0_{C,k+1} - \varphi^0_{C,k}}{h} - Cv_{C,0} + \hat{q}(\varphi^0_{M,k} + \varphi_{M,0}) - \hat{q}(\varphi_{M,0}) = 0.$$

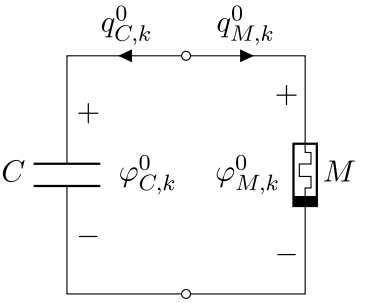

Fig. 3. Discrete-time MC circuit in the flux–charge domain.

Taking into account that KφL reads as $\varphi^0_{C,k} = \varphi^0_{M,k}$, we obtain the first-order map in the state variable $\varphi^0_{C,k}$,

$$\varphi^0_{C,k+1} = \varphi^0_{C,k} - \frac{h}{C}(\hat{q}(\varphi^0_{C,k} + \varphi_{M,0}) - \hat{q}(\varphi_{M,0})) + hv_{C,0}$$

or

$$\varphi^0_{C,k+1} = \varphi^0_{C,k} - \frac{h}{C}\hat{q}(\varphi^0_{C,k} + \varphi_{M,0}) + \frac{h}{C}Q_0, \tag{17}$$

where

$$Q_0 = w(v_C(t_0), \varphi_M(t_0)) = Cv_{C,0} + \hat{q}(\varphi_{M,0})$$

is the manifold index depending on the initial conditions $v_{C,0}, \varphi_{M,0}$ for the state variables in the VCD. The initial condition for the first-order map is $\varphi^0_{C,0} = 0$.

The map can be rewritten as

$$\varphi^0_{M,k+1} = \varphi^0_{M,k} - \frac{h}{C}\hat{q}(\varphi^0_{M,k} + \varphi_{M,0}) + \frac{h}{C}Q_0$$

or, equivalently,

$$\varphi_{M,k+1} = \varphi_{M,k} - \frac{h}{C}\hat{q}(\varphi_{M,k}) + \frac{h}{C}Q_0. \tag{18}$$

Let $(v_{C,k}, \varphi_{M,k})$, $k = 1, 2, \ldots$, be the solution of the second-order map (16) in the VCD with the initial conditions $v_{C,0}, \varphi_{M,0}$. It can be checked that $\varphi_{M,k}$, $k = 0, 1, 2, \ldots$, is the solution of the first-order map (18) in the FCD with the initial condition $\varphi_{M,0}$, provided $Q_0 = Cv_{C,0} + \hat{q}(\varphi_{M,0})$. Conversely, given Q_0, if $\varphi_{M,k}$, $k = 0, 1, 2, \ldots$, is the solution of (18) with the initial condition $\varphi_{M,0}$, then $((\varphi_{M,k+1} - \varphi_{M,k})/h, \varphi_{M,k})$ is the solution of (16) with the initial conditions $v_{C,0} = (Q_0 - \hat{q}(\varphi_{M,0}))/C$, $\varphi_{M,0}$.

4.4. *Coexisting attractors and flip bifurcations without parameters*

We have seen that the DT MC circuit is defined by the second-order map (16) in the VCD. However, the state space in the VCD is foliated in the one-dimensional invariant manifolds and on each manifold, the circuit is defined by the first-order map (18). If we let $x(t) = \varphi_M(t)$, and also let for simplicity $C = 1$, then this map can be rewritten as

$$x_{k+1} = x_k - h\hat{q}(x_k) + hQ_0, \tag{19}$$

with $x_0 = \varphi_{M,0}$. Thus, we obtained ∞^1 different first-order maps, in one-to-one correspondence with the manifolds. Each map differs from the others due to the additive term hQ_0 depending on the manifold index Q_0, i.e. on the initial conditions for the state variables in the VCD.

Assume the memristor has the typical nonlinearity $\hat{q}(\varphi_M) = a_M\varphi_M + b_M\varphi_M^3$, where a_M, b_M are fixed real numbers. Then, the map (19) becomes

$$x_{k+1} = x_k - h(a_M x_k + b_M x_k^3) + hQ_0, \tag{20}$$

and it depends upon the step size h and the manifold index Q_0. For this map, we can envisage two conceptually different types of bifurcations:

(1) Standard bifurcations due to varying parameter h for a fixed manifold index Q_0. In this regard, it is of importance to stress that, as discussed before, changing h does not alter the foliation in invariant manifolds of the state space of the MC circuit and does not change the invariant manifolds themselves. This fundamental property enables us to use the step size h as a bifurcation parameter while maintaining fixed the foliation and structure of invariant manifolds.
(2) Bifurcations due to varying the initial conditions in the VCD and the manifold index Q_0 for the fixed parameter h. In analogy to what happens for CT circuits, this special type of bifurcations is referred to as bifurcations without parameters [Corinto & Forti, 2017].

Suppose for simplicity that $a_M = 0$ and $b_M = 1$, i.e. $q_M = \hat{q}(\varphi_M) = \varphi_M^3$. Using a standard notation, the map (20) is defined by

$$x \to f(x) = x - hx^3 + hQ_0. \tag{21}$$

The fixed points $\overline{x}$ of the map satisfy $f(\overline{x}) = \overline{x}$. Note that, for any $Q_0 \in \mathbb{R}$, the map has a unique fixed point

$$\overline{x} = Q_0^{1/3}.$$

The change of variable $y = x - Q_0^{1/3}$ yields the map

$$y \to F(y) = y - hy^3 - 3hy^2Q_0^{1/3} - 3hyQ_0^{2/3}$$

which has a unique fixed point at $\overline{y} = 0$. The partial derivative of F with respect to y is given by

$$F_y(y) = 1 - 3hy^2 - 6hyQ_0^{1/3} - 3hQ_0^{2/3},$$

so that

$$F_y(0) = 1 - 3hQ_0^{2/3}.$$

It is easy to check that we have $|F'(0)| < 1$, hence the fixed point $\overline{y} = 0$ is asymptotically stable (AS), provided $Q_0 \neq 0$ and $h < (2/3)|Q_0|^{-2/3}$. Moreover, we can verify geometrically via the stair-step diagram that $\overline{y} = 0$ is AS for any h, when $Q_0 = 0$. When $h > (2/3)|Q_0|^{-2/3}$, we have $|F'(0)| > 1$ and so the fixed point $\overline{y}$ is unstable. The region in the (h, Q_0)-plane where the fixed point is AS (resp., unstable) is denoted by R_S (resp., R_U) and is shown in Fig. 4.

The condition for which the map defined by F displays a flip bifurcation at $y = 0$ when varying the parameter h or parameter Q_0 is given by $F_y(0) = -1$ [Kuznetsov, 1998], i.e.

$$hQ_0^{2/3} = \frac{2}{3}.$$

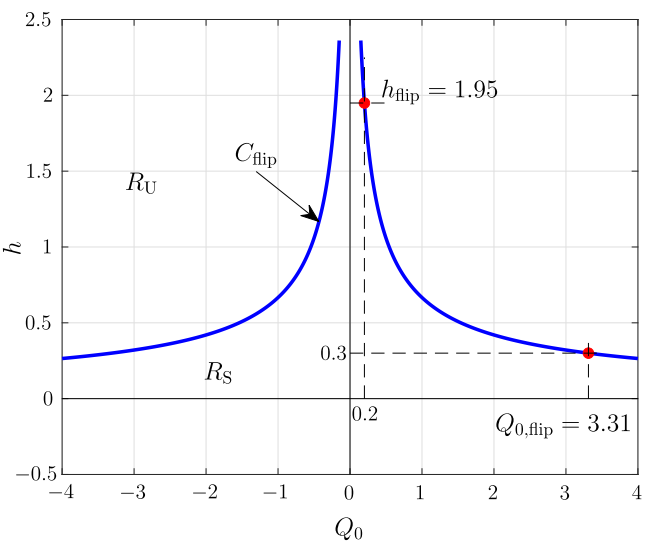

Fig. 4. Flip bifurcation curve C_{flip} and the region R_S (resp., R_U) where the fixed point $\overline{x}$ of the map (21) is AS (resp., unstable).

This defines the curve C_{flip} in the (h, Q_0)-plane shown in Fig. 4. Solving for h, we obtain

$$C_{\text{flip}} = \left\{(h, Q_0) : Q_0 \neq 0, h = h_{\text{flip}} \doteq \left(\frac{2}{3}\right) Q_0^{-2/3}\right\},$$

while there is no solution h when $Q_0 = 0$. Solving for Q_0, we obtain

$$C_{\text{flip}} = \left\{(h, Q_0) : Q_0 = Q_{0,\text{flip}} \doteq \left(\frac{2}{3h}\right)^{3/2}\right\} \cup \{(h, Q_0) : Q_0 = -Q_{0,\text{flip}}\}.$$

Note that C_{flip} is the boundary between R_S and R_U.

Let us now study in more detail the bifurcations with respect to h for fixed Q_0, i.e. on a given manifold $\mathcal{M}(Q_0)$ for the map $y \to F(y)$. We have already seen that if $Q_0 = 0$, the fixed point $\overline{y} = 0$ is AS for any h. We then consider the case $Q_0 \neq 0$ and suppose without loss of generality $Q_0 > 0$. The value of h for which there is a flip bifurcation is $h_{\text{flip}} = (2/3)Q_0^{-2/3}$. The change of variable $\eta = h - (2/3)Q_0^{-2/3}$ yields the map

$$y \to H(y, \eta) = y - \left(\eta + \left(\frac{2}{3}\right) Q_0^{-2/3}\right) \times (y^3 + 3y^2 Q_0^{1/3} + 3y Q_0^{2/3})$$

which has a flip bifurcation at $\eta = 0$. In order that the bifurcation is generic, the two following transversality conditions need to be satisfied [Kuznetsov, 1998]:

(B.1) $$c_0 \doteq \frac{1}{2} H_{yy}(0,0)^2 + \frac{1}{3} H_{yyy}(0,0) \neq 0;$$

(B.2) $$H_{y\eta}(0,0) \neq 0.$$

Some simple computations yield

$$c_0 = \frac{20}{3} Q_0^{-2/3} > 0;$$

since $Q_0 \neq 0$, hence (B.1) is satisfied. Moreover, we have

$$H_{y\eta}(0,0) = -3Q_0^{2/3} < 0;$$

since $Q_0 \neq 0$, hence (B.2) is also satisfied. We remark that, since $c_0 > 0$ for any $Q_0 > 0$, the flip bifurcation is supercritical and a stable period-two cycle bifurcates at the fixed point for $h > h_{\text{flip}}$ [Kuznetsov, 1998]. An analogous result is obtained for $Q_0 < 0$.

Let us now study the bifurcations with respect to Q_0 for fixed h. The values of Q_0 for which there is a flip bifurcation at a given h are $\pm Q_{0,\text{flip}}$, where $Q_{0,\text{flip}} = (2/3h)^{3/2}$. Consider without loss of generality $Q_0 = (2/3h)^{3/2}$. The change of variables $\mu = Q_0 - (2/3h)^{3/2}$ yields the map

$$y \to Q(y, \mu) = y - hy^3 - 3hy^2\left(\mu + \left(\frac{2}{3h}\right)^{3/2}\right)^{1/3} - 3hy\left(\mu + \left(\frac{2}{3h}\right)^{3/2}\right)^{2/3}$$

which has a flip bifurcation at $\mu = 0$. It can be checked that

$$c_0 = \frac{1}{2} Q_{yy}(0,0)^2 + \frac{1}{3} Q_{yyy}(0,0) = 10h > 0;$$

since $h > 0$, hence (B.1) is satisfied. We also have

$$Q_{y\mu}(0,0) = -\sqrt{6} h^{3/2} < 0;$$

since $h > 0$, hence (B.2) is also satisfied. Since $c_0 > 0$ for any $h > 0$, the flip bifurcation is supercritical and a stable period-two cycle bifurcates for $Q > Q_{0,\text{flip}}$ at the fixed point [Kuznetsov, 1998]. An analogous result is obtained for $Q_0 = -(2/3h)^{3/2}$.

Let us illustrate these behaviors using the numerical simulations of the map (21). First consider the bifurcations with respect to h for fixed Q_0. If $Q_0 = 0$, from simulations (not reported here) we observed convergence to the AS fixed point $\overline{x} = 0$ for any h. Then, choose $Q_0 = 0.2$, hence $h_{\text{flip}} = 1.95$ (cf. Fig. 4). Figure 5 depicts the bifurcation diagram obtained with MATLAB. It is seen that for $0 < h < h_{\text{flip}}$ the solution converges to the AS fixed point $\overline{x} = Q_0^{1/3} = 0.585$. For $h > h_{\text{flip}}$, as predicted, the fixed point becomes unstable and we observe an attracting cycle of period two, confirming that we have a supercritical flip bifurcation at h_{flip}. By further increasing h, the cycle undergoes a second flip bifurcation at $h = 2.44$ with the birth of a cycle of period four. Then, we have a typical scenario where we observe a cascade of flip bifurcations accumulating at $h = 2.61$ where there is the birth of a complex attractor.

Then, let us fix $h = 0.3$. We have $Q_{0,\text{flip}} = \pm 3.31$ (cf. Fig. 4). Suppose we start with $Q_0 = 0$ and we increase Q_0. The corresponding bifurcation diagram is depicted in Fig. 6. It is seen that the solution converges to the AS fixed point $\overline{x} = Q_0^{1/3}$,

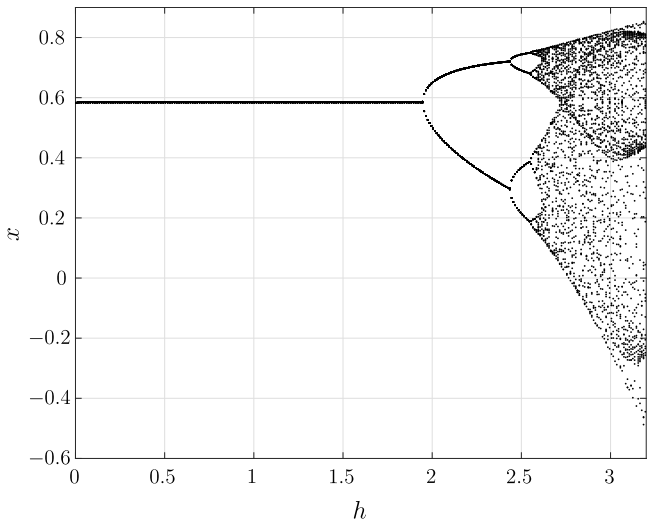

Fig. 5. Bifurcation diagram of the map (21) when $Q_0 = 0.2$ and the step size h is varied.

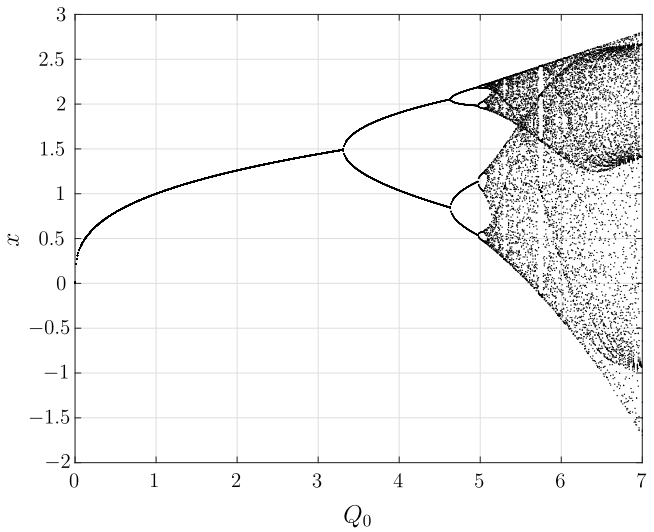

Fig. 6. Bifurcation diagram of the map (21) when $h = 0.3$ and parameter Q_0 is varied.

depending on Q_0, as long as $0 \leq Q_0 < Q_{0,\text{flip}}$. Then, as predicted, for $Q_0 > 0$ the fixed point becomes unstable and we observe an attracting cycle of period two, confirming that there is a supercritical flip bifurcation at $Q_{0,\text{flip}}$. At $Q_0 = 4.65$, we observe a second flip with the birth of a cycle of period four, followed by a cascade of flip bifurcations and the birth of a chaotic attractor at $Q_0 = 5.11$. A similar scenario is observed if we decrease Q_0 starting from $Q_0 = 0$.

5. Discussion

In this section, we provide some comments on the rich dynamic behavior we can observe in a DT MC circuit. This is related to two main reasons. The first reason is the foliation of the state space in invariant manifolds and the coexistence of infinitely many different dynamics and attractors. The second reason is that the previous property holds for any discretization step size and it is known that an intrinsic property of DT systems is to display richer dynamics than their CT counterparts when the step size is varied.

Let us first consider the complexities related to the decomposition in invariant manifolds. Consider the second-order map (16) of the DT MC circuit in the VCD. Suppose once again that $\hat{q}(\varphi_M) = \varphi_M^3$ and let $y_k = v_{C,k}$ and $z_k = \varphi_{M,k}$. The map can be written as

$$\begin{pmatrix} y \\ z \end{pmatrix} \to \begin{pmatrix} f_1(y,z) \\ f_2(y,z) \end{pmatrix} = \begin{pmatrix} y - (z+hy)^3 + z^3 \\ z + hy \end{pmatrix}. \tag{22}$$

It can be checked that there is a line of nonisolated fixed points given by $(\overline{y}, \overline{z}) = (0, \zeta)$, where $\zeta \in \mathbb{R}$. Note that all fixed points are characterized by a capacitor voltage equal to 0, while the memristor flux can assume any value. Now, suppose as it was done previously that the step size is fixed at $h = 0.3$. It follows that the second-order map (22) embeds all the different dynamics displayed by the first-order map (21) when varying Q_0 (cf. Fig. 6). To see this more clearly, consider Fig. 7, where we have shown in the state space (y, z) of (22)

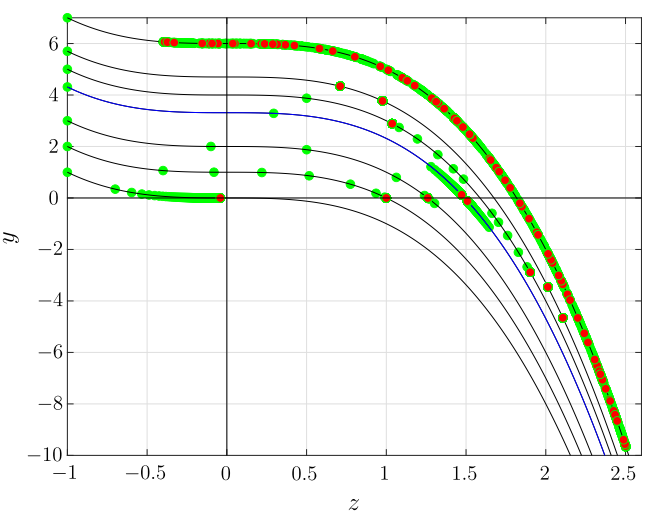

Fig. 7. From left to right: Invariant manifolds $\mathcal{M}(Q_0)$, where $Q_0 \in \{0, 1, 2, 3.31, 4, 4.7, 6\}$, for the second-order map (22). For each manifold, the figure shows with green points the solution starting on the manifold at $z_0 = -1$. The red points represent the long-term behavior of each solution.

a number of different invariant manifolds $\mathcal{M}(Q_0)$ obtained by varying Q_0. Note that each manifold is given by $y = Q_0 - z^3$. For each manifold, the figure shows the trajectory starting at the initial condition on the manifold with $z_0 = -1$. It can be checked that, as predicted by the theory, each manifold is invariant for the dynamics of (22), i.e. the solution starting on a manifold stays on it for all $k > 0$. Moreover, in the figure, we have shown for each manifold the long-term behavior of the solution and the corresponding attractor. It is seen that when $Q_0 = 0$ the solution converges monotonically to the fixed point $(0, 0)$. When $Q_0 = 1 < Q_{0,\text{flip}} = 3.31$, we observe again monotonic convergence to the fixed point $(0, \overline{x} = Q_0^{1/3} = 1)$. If $Q_0 = 2$, we have convergence to the fixed point $(0, 2^{1/3})$, but in this case the solution approaches the fixed point by oscillating around it. An analogous situation is observed when $Q_0 = Q_{0,\text{flip}} = 3.31$. Then, when $Q_0 = 4$, we have convergence to a period-two cycle, while when $Q_0 = 4.7$, there is convergence to a period-four cycle. Finally, when $Q_0 = 6$, we observe convergence to a complex attractor. In Fig. 8, we provide an alternate 3D visualization of these behaviors using an additional axis Q_0. All these different asymptotic dynamics, i.e. convergent, periodic and complex dynamics, coexist for the same set of circuit parameters of the map (22). In a more suggestive way, suppose we increase Q_0 and we move along the line of fixed points in Fig. 7. Then, it is seen that at $Q_{0,\text{flip}} = 3.31$ the fixed point with $\overline{x} = Q_{0,\text{flip}}^{1/3} = 1.49$ undergoes a (supercritical) flip bifurcation without parameters. Moreover, at $Q_0 = 4.65$, the period-two cycle undergoes a second flip bifurcation without parameters and so on. In this way, we have given a rigorous proof of the coexistence of infinitely many different attractors, and the existence of flip bifurcations without parameters, for the second-order DT MC circuit (22).

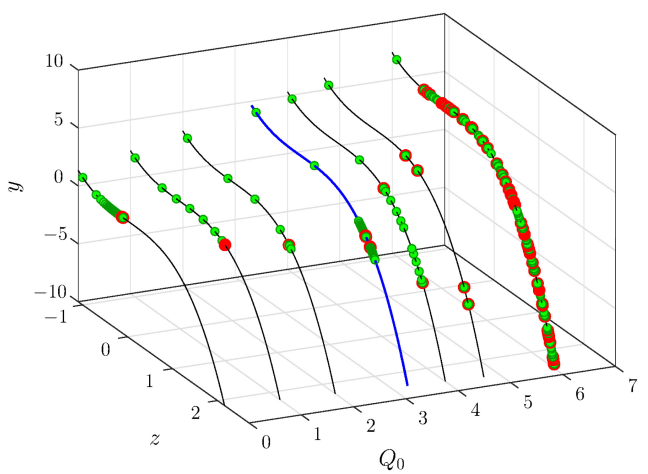

Fig. 8. An alternate 3D visualization of the coexisting dynamics for the second-order map (22).

Consider now the complexities due to changing the discretization step size on a given manifold. We have already seen in Fig. 5 that by increasing h the DT MC circuit can pass on a given invariant manifold from a simple convergent dynamics to periodic and even complex dynamics. Such a scenario is typical of many discretization schemes of CT systems. The complexities due to varying h add to those due to changing the invariant manifold via the initial conditions for the MC CT circuit in the VCD.

As a final comment, let us compare the behavior of the DT MC circuit with that of its CT counterpart. A CT MC satisfies in the VCD the second-order ODE (1). It is easy to see that on an invariant manifold $\mathcal{M}(Q_0)$ the memristor flux satisfies (FCD) the first-order ODE

$$\dot{\varphi}_M = -\hat{q}(\varphi_M) + Q_0 = -\varphi_M^3 + Q_0. \qquad (23)$$

We refer the reader to Corinto and Forti [2016] for more details. It is seen that, for any initial condition $\varphi_{M,0}$, the solution of (23) converges to the equilibrium point $\overline{x} = Q_0^{1/3}$. Hence, (1) always displays convergent dynamics and no bifurcations without parameters of the equilibrium point are present. Quite differently, we have seen that the second-order DT MC map can embed infinitely many convergent, periodic and also complex dynamics and it can display flip bifurcations.

6. Analysis of MRLC Circuit via DT-FCAM

6.1. *Analysis in the VCD*

Consider the CT MRLC circuit in the class $\mathcal{LM}$, with an ideal resistor $R > 0$, an ideal capacitor $C > 0$, an ideal inductor $L > 0$ and an ideal flux-controlled memristor $q_M = \hat{q}_M(\varphi_M)$, shown in Fig. 9. The circuit is obtained by replacing the nonlinear resistor in a Murali–Lakshmanan–Chua circuit [Ishaq Ahamed & Lakshmanan, 2013] with a memristor.

Let us analyze the corresponding DT MRLC circuit in Fig. 10 using DT-FCAM and the new discretization scheme introduced for the memristor.

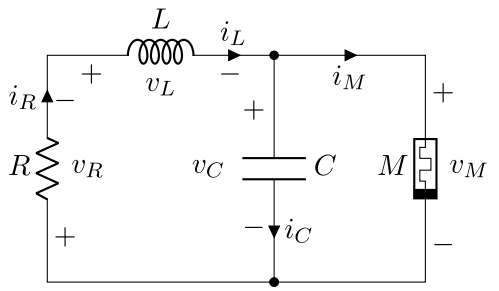

Fig. 9. Continuous-time MRLC circuit.

In the VCD, the KCL reads as

$$i_{L,k} = i_{C,k} + i_{M,k},$$

while the two KVLs can be written as

$$v_{R,k} + v_{L,k} + v_{C,k} = 0$$

and

$$v_{M,k} = v_{C,k}.$$

Using the CRs of circuit elements, the above equations can be written as

$$i_{L,k} = C\frac{v_{C,k+1} - v_{C,k}}{h} + \frac{\hat{q}(\varphi_{M,k+1}) - \hat{q}(\varphi_{M,k})}{h},$$

$$Ri_{i_{L,k}} + L\frac{i_{L,k+1} - i_{L,k}}{h} + v_{C,k} = 0,$$

$$\varphi_{M,k+1} = \varphi_{M,k} + hv_{C,k}.$$

These yield the third-order map in the VCD describing the dynamics of the MRLC circuit,

$$\begin{cases} v_{C,k+1} = v_{C,k} - \dfrac{\hat{q}(\varphi_{M,k} + hv_{C,k}) - \hat{q}(\varphi_{M,k})}{C} \\ \qquad\qquad + \dfrac{h}{C}i_{L,k}, \\ i_{L,k+1} = \left(1 - \dfrac{Rh}{L}\right) i_{i_{L,k}} - \dfrac{h}{L}v_{C,k}, \\ \varphi_{M,k+1} = \varphi_{M,k} + hv_{C,k}. \end{cases} \tag{24}$$

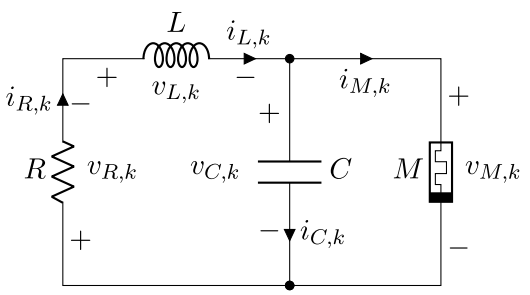

Fig. 10. Discrete-time MRLC circuit.

The state variables are $v_{C,k}, i_{L,k}, \varphi_{M,k}$ and the initial conditions are $v_{C,0} = v_C(t_0), i_{L,0} = i_L(t_0)$, $\varphi_{M,0} = \varphi_M(t_0)$.

6.2. *First integral and invariant manifolds*

From the second equation in (24), we obtain

$$i_{L,k+1} - i_{L,k} = -\frac{Rh}{L}i_{L,k} - \frac{h}{L}v_{C,k},$$

and using the third equation,

$$hi_{L,k} = -\frac{L}{R}(i_{L,k+1} - i_{L,k}) - \frac{1}{R}(\varphi_{M,k+1} - \varphi_{M,k}).$$

Substituting in the first equation and rearranging, we have

$$Cv_{C,k+1} + \hat{q}(\varphi_{M,k+1}) + \frac{L}{R}i_{L,k+1} + \frac{1}{R}\varphi_{M,k+1}$$
$$= Cv_{C,k} + \hat{q}(\varphi_{M,k}) + \frac{L}{R}i_{L,k} + \frac{1}{R}\varphi_{M,k}.$$

Consider the function of the state variables

$$w(v_C, i_L, \varphi_M) = Cv_C + \frac{Li_L}{R} + \hat{q}(\varphi_M) + \frac{\varphi_M}{R}.$$

We have shown that

$$w(v_{C,k+1}, i_{L,k+1}, \varphi_{M,k+1}) = w(v_{C,k}, i_{L,k}, \varphi_{M,k})$$

along the solutions of (24). Hence, w is a first integral for the DT RLMC circuit and it coincides with that of the CT MC circuit (cf. Corinto *et al.* [2021, Chapter 6]). Note that this property holds for any step size h.

Now, introduce the subsets of the state space

$$\mathcal{M}(Q_0) = \Big\{(v_C, i_L, \varphi_M) \in \mathbb{R}^3 : w(v_C, i_L, \varphi_M)$$
$$= Cv_C + \frac{Li_L}{R} + \hat{q}(\varphi_M) + \frac{\varphi_M}{R} = Q_0\Big\}, \tag{25}$$

where $Q_0 \in \mathbb{R}$. Each set is a two-dimensional *invariant manifold* for the dynamics of (16) and it is uniquely defined by the *manifold index*

$$Q_0 = Cv_{C,0} + \frac{Li_{L,0}}{R} + \hat{q}(\varphi_{M,0}) + \frac{\varphi_{M,0}}{R}$$

depending upon the initial conditions of the state variables in the VCD.

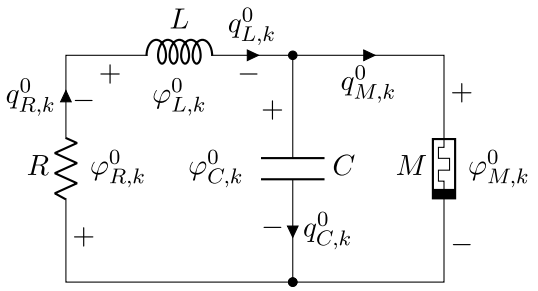

Fig. 11. Discrete-time MRLC circuit in the flux–charge domain.

Once again, we note that the first integral w and the invariant manifolds are independent of the step size h.

6.3. *Analysis in the FCD*

Let us now analyze the DT MRLC circuit of Fig. 11 in the FCD to determine the dynamics on each invariant manifold. KqL yields

$$q^0_{L,k} = q^0_{C,k} + q^0_{M,k},$$

and using the CRs of circuit elements,

$$q^0_{L,k} = C\frac{\varphi^0_{C,k+1} - \varphi^0_{C,k}}{h} - Cv_{C,0} + \hat{q}(\varphi^0_{M,k} + \varphi_{M,0}) - \hat{q}(\varphi_{M,0}).$$

Moreover, from KφL we have

$$\varphi^0_{R,k} + \varphi^0_{L,k} + \varphi^0_{C,k} = 0,$$

and so

$$Rq^0_{L,k} + L\frac{q^0_{L,k+1} - q^0_{L,k}}{h} - Li_{L,0} + \varphi^0_{C,k} = 0.$$

Finally, from KφL we obtain

$$\varphi^0_{M,k} = \varphi^0_{C,k}.$$

Therefore, we obtain the second-order map describing the dynamics of the MRLC circuit in the FCD,

$$\begin{cases} \varphi^0_{C,k+1} = \varphi^0_{C,k} - \dfrac{h}{C}(\hat{q}(\varphi^0_{C,k} + \varphi_{M,0}) - \hat{q}(\varphi_{M,0})) \\ \qquad\qquad + \dfrac{h}{C}q^0_{L,k} + hv_{C,0}, \\ q^0_{L,k+1} = \left(1 - \dfrac{Rh}{L}\right) q^0_{L,k} - \dfrac{h}{L}\varphi^0_{C,k} + hi_{L,0}. \end{cases} \tag{26}$$

The state variables are $\varphi^0_{C,k}, q^0_{L,k}$ and the initial conditions are $\varphi^0_{C,0} = 0, q^0_{L,0} = 0$.

6.4. *Coexisting attractors and Poincaré–Andronov–Hopf bifurcations without parameters*

Letting $x_k = \varphi_{M,k}$, $y_k = q^0_{L,k} - \varphi_{M,0}/R - Li_{L,0}/R$, we obtain from (26) a second-order map that can be rewritten as

$$\begin{pmatrix} x \\ y \end{pmatrix} \to \begin{pmatrix} f_1(x,y) \\ f_2(x,y) \end{pmatrix} = \begin{pmatrix} x + \dfrac{h}{C}y - \dfrac{h}{C}\hat{q}(x) + \dfrac{h}{C}Q_0 \\ y - \dfrac{hR}{L}y - \dfrac{h}{L}x \end{pmatrix}. \tag{27}$$

As it was done for the MC circuit, let us illustrate the dynamics and bifurcations of (27) in the case where the memristor nonlinearity is chosen as $\hat{q}(x) = x^3$. The fixed points $(\overline{x}, \overline{y})$ of the map satisfy

$$\frac{\overline{x}}{R} + \overline{x}^3 = Q_0$$

and $\overline{y} = -\overline{x}/R$. For any $Q_0 \in \mathbb{R}$, there is a unique fixed point $(\overline{x}(Q_0), -\overline{x}(Q_0)/R)$, where $\overline{x}(Q_0)$ is a strictly monotone increasing function of Q_0. The change of variables $X = x - \overline{x}(Q_0)$, $Y = y + \overline{x}(Q_0)/R$ yields the map with a unique fixed point at $(\overline{X}, \overline{Y}) = (0,0)$,

$$\begin{pmatrix} X \\ Y \end{pmatrix} \to \begin{pmatrix} F_1(X,Y,h,Q_0) \\ F_2(X,Y,h,Q_0) \end{pmatrix} = \begin{pmatrix} X + \dfrac{h}{C}Y - \dfrac{3h}{C}\overline{x}(Q_0)^2 X - \dfrac{h}{C}X^3 - \dfrac{3h}{C}\overline{x}(Q_0)X^2 \\ Y - \dfrac{h}{L}X - \dfrac{hR}{L}Y \end{pmatrix}. \tag{28}$$

We want to study the possible existence of Poincaré–Andronov–Hopf (PAH) bifurcations for the second-order map when varying the parameter h or Q_0. The Jacobian of the map evaluated at $(0,0)$ is

$$J = \begin{pmatrix} 1 - \dfrac{3h\overline{x}^2(Q_0)}{C} & \dfrac{h}{C} \\ -\dfrac{h}{L} & 1 - \dfrac{hR}{L} \end{pmatrix}.$$

We suppose henceforth that the circuit parameters satisfy

$$R < 2\sqrt{\frac{L}{C}}, \tag{29}$$

and that $|Q_0|$ is sufficiently small in order that the following condition holds:

$$R^2 - 4\frac{L}{C} - \frac{6LR\overline{x}^2(Q_0)}{C} + \frac{9L^2\overline{x}^4(Q_0)}{C^2} < 0. \tag{30}$$

Under (30), the eigenvalues $\lambda_{1,2} = \alpha \pm j\beta$ of J are complex conjugates with $\beta \neq 0$, hence

$$\lambda_1\lambda_2 = \alpha^2 + \beta^2 = \det(J)$$

and

$$|\lambda_1|^2 = |\lambda_2|^2 = \det(J).$$

It can be seen that we have

$$\det(J) = 1,$$

i.e. λ_1, λ_2 are on the unit circle of the complex plane if

$$h = \frac{RC + 3L\overline{x}(Q_0)^2}{1 + 3R\overline{x}(Q_0)^2}. \tag{31}$$

This defines a curve in the (h, Q_0)-plane where a PAH bifurcation occurs, namely,

$$C_{\mathrm{PAH}} = \left\{ (h, Q_0) : h = h_{\mathrm{PAH}}(Q_0) \doteq \frac{RC + 3L\overline{x}(Q_0)^2}{1 + 3R\overline{x}(Q_0)^2} \right\} \tag{32}$$

for any $Q_0 \in \mathbb{R}$. Given any $h > 0$, we can also solve for Q_0 and obtain two values $\pm Q_{0,\mathrm{PAH}}(h)$ for which (31) is satisfied.

Let us study in more detail the bifurcations when h is varied for a fixed Q_0, i.e. the bifurcations on a fixed invariant manifold $\mathcal{M}(Q_0)$. In order to verify that a generic PAH bifurcation occurs, we resort to verifying the conditions (i)–(iv) and an additional transversality condition in Hale and Koçak [1991, Theorem 15.31]. Condition (i), which amounts to $F_1(0,0,h,Q_0) = 0$ and $F_2(0,0,h,Q_0) = 0$ for h close to $h_{\mathrm{PAH}}(Q_0)$, is satisfied by construction. Condition (ii) requires that J has complex eigenvalues $\alpha \pm j\beta$ such that $|\alpha \pm j\beta| = 1$ when $h = h_{\mathrm{PAH}}(Q_0)$, which is true by construction; moreover, we have $\beta \neq 0$ for h close to $h_{\mathrm{PAH}}(Q_0)$, which is true for continuity under (29) and (30). For the transversality condition (iii), we have to check that the eigenvalues of J cross the unit circle when varying the parameter h through the critical value $h_{\mathrm{PAH}}(Q_0)$. We have

$$\begin{aligned} \sigma(Q_0) &\doteq \left.\frac{\partial \det(J)}{\partial h}\right|_{h=h_{\mathrm{PAH}}(Q_0)} \\ &= \frac{1}{LC}(2h_{\mathrm{PAH}}(Q_0) - CR - 3L\overline{x}(Q_0)^2 \\ &\quad + 6Rh_{\mathrm{PAH}}\overline{x}(Q_0)^2), \end{aligned} \tag{33}$$

hence condition (iii) is met provided $\sigma(Q_0) \neq 0$.

Consider now the eigenvalues of J when $h = h_{\mathrm{PAH}}(Q_0)$,

$$\begin{aligned} \overline{\lambda}_{1,2} = \overline{\alpha} \pm j\overline{\beta} = &-\frac{3Lh_{\mathrm{PAH}}(Q_0)\overline{x}(Q_0)^2 - 2CL + CRh_{\mathrm{PAH}}(Q_0)}{2CL} \\ &\pm j\frac{h_{\mathrm{PAH}}(Q_0)\sqrt{4CL - C^2R^2 + 6CLR\overline{x}(Q_0)^2 - 9L^2\overline{x}(Q_0)^4}}{2CL}. \end{aligned} \tag{34}$$

Condition (iv) requires that $\overline{\lambda}_1^k \neq 1$, $k = 1,2,3,4$. Since $\overline{\beta} \neq 0$, we need to have $\overline{\alpha} \neq 0$ and if $\overline{\alpha} < 0$, then $\overline{\beta}/\overline{\alpha} \neq \pm\sqrt{3}$.

Finally, the last relevant transversality condition concerns the coefficient a appearing in formula (15.23) of the quoted theorem, that needs to be different from 0. This coefficient characterizes the type of PAH bifurcation. More precisely, if $a > 0$, then the bifurcation is supercritical and (28) has a unique stable closed invariant curve encircling the fixed point $(0,0)$ that bifurcates at $h_{\mathrm{PAH}}(Q_0)$ from this point and exists for sufficiently small

$h - h_{\mathrm{PAH}}(Q_0) > 0$. If instead we have $a < 0$, then (28) has a unique unstable closed invariant curve around the fixed point $(0, 0)$ that shrinks at $h_{\mathrm{PAH}}(Q_0)$ to this point and exists for sufficiently small $h - h_{\mathrm{PAH}}(Q_0) < 0$.

The condition on a is typically the most elaborate to check. For illustration purposes, we first consider the relatively simple situation where $Q_0 = 0$, i.e. the dynamics evolves on the manifold $\mathcal{M}(0)$, and, from (31), we simply have $h_{\mathrm{PAH}}(0) = RC$. In this case, it is shown in Appendix A that the sought coefficient has the simple analytic expression

$$a(Q_0 = 0) = \frac{3R}{16}\left(2\frac{L}{C} - R^2 - R\right).$$

The general case $Q_0 \neq 0$ is illustrated by numerical means in the next example.

Example 6.1. Choose $R = 1, C = 1$ and $L = 5$. In this case, we have that (30) is satisfied for $|Q_0| < 0.82$. Figure 12 shows the curve C_{PAH} in (32), while Fig. 13 shows $\sigma(Q_0)$. Since $\sigma(Q_0) > 0$, condition (iii) is satisfied for any Q_0; moreover, the eigenvalues of J cross the unit circle from inside to outside when increasing h through $h_{\mathrm{PAH}}(Q_0)$. It can be checked that we have $|\lambda_{1,2}| < 1$ (resp., $|\lambda_{1,2}| > 1$), i.e. the fixed point is AS (resp., unstable) in the region R_S (resp., R_U) in Fig. 12. Note that C_{PAH} is the boundary between R_S and R_U. Now, suppose $Q_0 = 0$, in which case $h_{\mathrm{PAH}}(0) = CR = 1$. It has been checked numerically on the basis of (34) that the nonresonance condition (iv) is satisfied provided

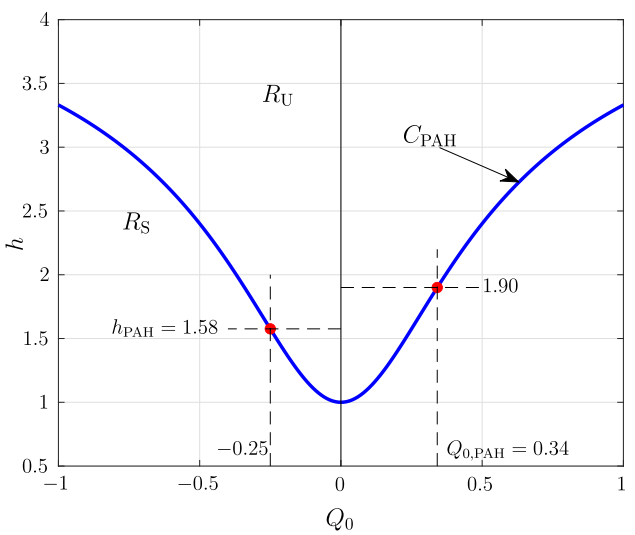

Fig. 12. Bifurcation curve C_{PAH} and region R_S (resp., R_U) where the fixed point $(\overline{x}, \overline{y})$ of the map (27) is AS (resp., unstable) when the circuit parameters are $C = 1, L = 5, R = 1$.

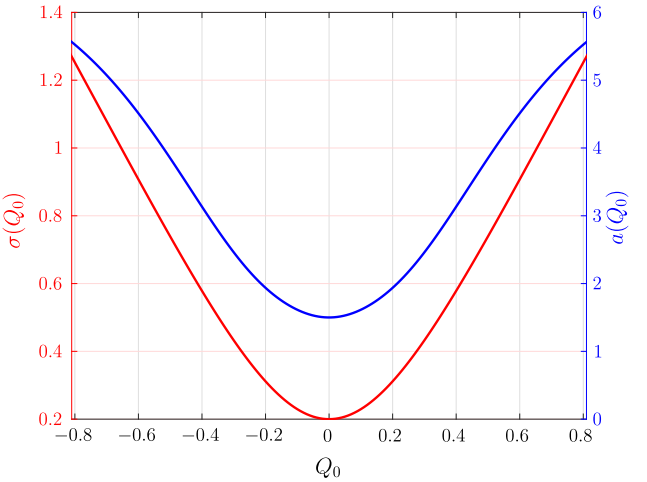

Fig. 13. Parameter $\sigma(Q_0)$ (red) and coefficient $a(Q_0)$ (blue) as a function of Q_0.

$h \neq 2.930$ and $h \neq 2.938$. Moreover, we have

$$a(Q_0 = 0) = \frac{3}{2},$$

hence on manifold $\mathcal{M}(0)$ we expect a generic supercritical PAH bifurcation at $h = h_{\mathrm{PAH}}(0) = 1$. This is confirmed by the bifurcation diagram shown in Fig. 14. We developed an algorithm based on Hale and Koçak [1991, Eq. (15.25)] to numerically evaluate the coefficient $a(Q_0)$ for any Q_0. The algorithm is quite involved and we omit the details to avoid an excessive length. Figure 13 shows $a(Q_0)$ in the interval $Q_0 \in [-0.82, 0.82]$. Once again, since $a(Q_0) > 0$ for any Q_0, we expect a generic supercritical PAH bifurcation when varying h for any Q_0 in the considered interval. For confirmation, Fig. 15 shows the bifurcation diagram in the case $Q_0 = -0.25$ and $h_{\mathrm{PAH}}(-0.25) = 0.341$.

Suppose now that h is fixed and we vary Q_0. Again, we use Hale and Koçak [1991, Theorem 15.31] to check if the PAH bifurcation is generic. It can be verified, as it was done previously, that conditions (i) and (ii) are satisfied, provided (29) and (30) hold. Moreover, we have

$$\frac{\partial \det(J)}{\partial \overline{x}(Q_0)} = \frac{6h\overline{x}(Q_0)}{C}\left(h\frac{R}{L} - 1\right)$$

and

$$\delta(h) \doteq \left.\frac{\partial \det(J)}{\partial Q_0}\right|_{Q_0 = \pm Q_{0,\mathrm{PAH}}} = \frac{6h\overline{x}(\pm Q_{0,\mathrm{PAH}})}{C}\overline{x}'(\pm Q_{0,\mathrm{PAH}})\left(h\frac{R}{L} - 1\right).$$

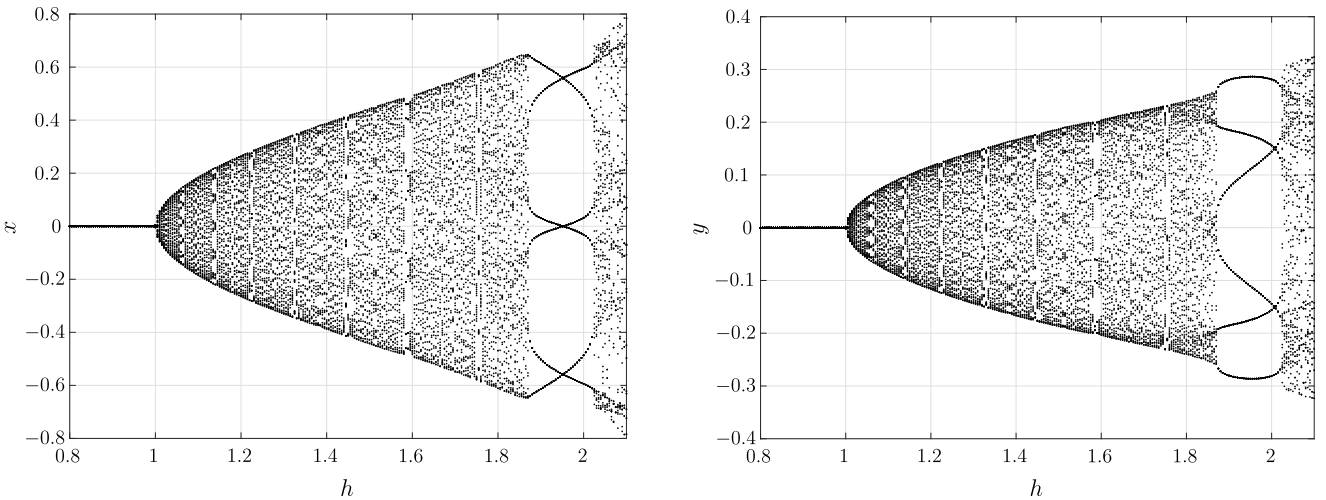

(a) (b)

Fig. 14. Bifurcation diagram of the map (27) with respect to h when $Q_0 = 0$: (a) variable x and (b) variable y.

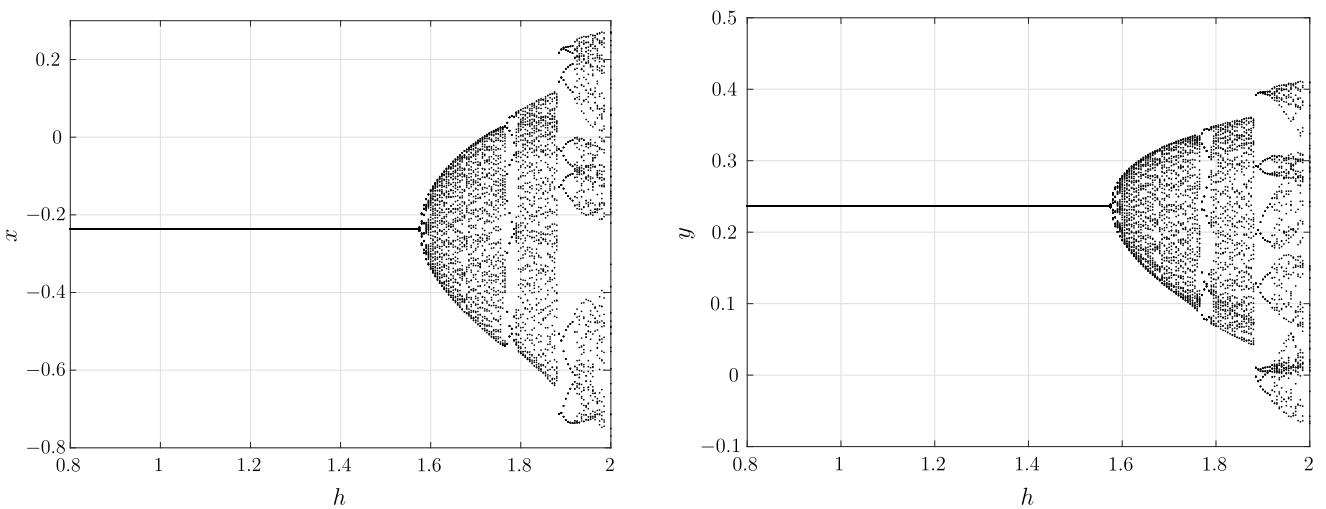

(a) (b)

Fig. 15. Bifurcation diagram of the map (27) with respect to h when $Q_0 = -0.25$: (a) variable x and (b) variable y.

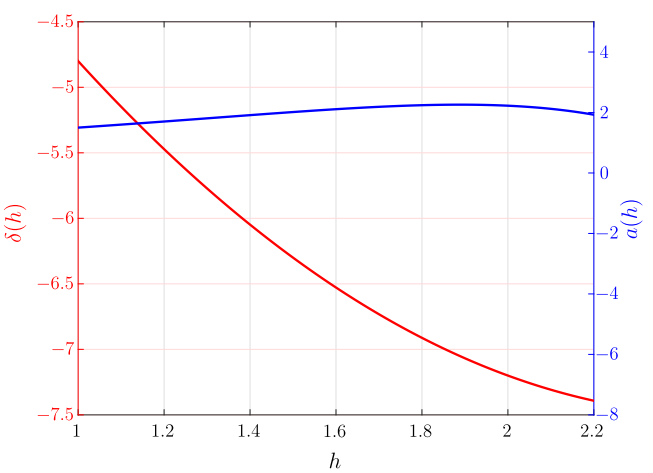

Fig. 16. Parameter $\delta(h)$ (red) and coefficient $a(h)$ (blue) for the second-order map (27).

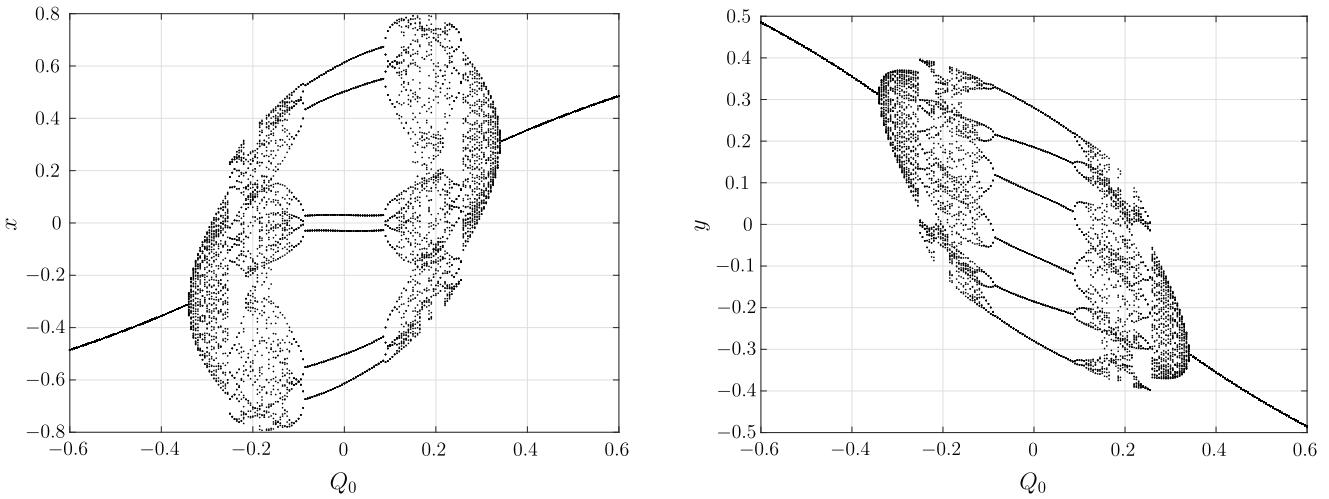

(a) (b)

Fig. 17. Bifurcation diagram of the map (27) with respect to Q_0 when $h = 1.9$: (a) Variable x and (b) variable y.

It is seen that $\sigma(h)$ does not vanish, i.e. condition (iii) is satisfied, when $Q_{0,\mathrm{PAH}} \neq 0$ and $h \neq L/R$.

The nonresonance condition (iv) and the transversality condition related to coefficient a are discussed in the next example.

Example 6.2. Consider again the second-order map in Example 6.1. On the basis of (34), it can be checked that the nonresonance condition (iv) is satisfied provided $Q_0 \neq \pm 0.537$, $Q_0 \neq \pm 0.542$ and $Q_0 \neq \pm 0.686$. Figure 16 shows $\delta(h)$ and $a(h)$ as a function of h. If we choose $h = 1.9$, we have $\delta(1.9) = -7.07 < 0$ at $-Q_{0,\mathrm{flip}} = -0.34$, while $\delta(1.9) = 7.07 > 0$ at $Q_{0,\mathrm{flip}} = 0.34$; moreover, $a(1.9) = 2.26 > 0$. Then, we expect a supercritical PAH without parameters at $-Q_{0,\mathrm{PAH}} = -0.34$ and an inverse supercritical PAH bifurcation without parameters at $Q_{0,\mathrm{PAH}} = 0.34$. This is indeed confirmed by the bifurcation diagram in Fig. 17. The diagram also shows quite a large interval $Q_0 \in [-0.085, 0.085]$ where the map displays a cycle of period six. It is worth noting that by increasing Q_0 the cycle undergoes a period-doubling bifurcation at $Q_0 = 0.085$ followed by a cascade of period-doubling bifurcations originating a complex attractor at $Q_0 = 0.12$.

7. Discussion

As it was done for the DT MC circuit, let us discuss the dynamic complexities due to the foliation of the state space in invariant manifolds. To this end, consider the third-order map (24) of the DT MRLC circuit in the VCD. Suppose once more that $\hat{q}(\varphi_M) = \varphi_M^3$ and let $r_k = v_{C,k}, s_k = i_{L,k}$ and $z_k = \varphi_{M,k}$. The map can be rewritten as

$$\begin{pmatrix} r \\ s \\ z \end{pmatrix} \rightarrow \begin{pmatrix} f_1(r,s,z) \\ f_2(r,s,z) \\ f_3(r,s,z) \end{pmatrix} = \begin{pmatrix} r - (z+hr)^3 + z^3 + hs \\ \left(1 - \dfrac{h}{5}\right) s - \dfrac{h}{5} r \\ z + hr \end{pmatrix}. \quad (35)$$

It is seen that the map has a line of nonisolated fixed points given by $(\overline{r}, \overline{s}, \overline{z}) = (0, 0, \xi)$, where $\xi \in \mathbb{R}$. Note that all fixed points are characterized by a capacitor voltage and an inductor current equal to 0, while the memristor flux can assume any value. If we suppose that the step size is fixed at $h = 1.9$, the third-order map (35) embeds all the different dynamics displayed by the second-order map (27) when varying Q_0 (cf. Fig. 17). In Fig. 18, we have shown a number of different invariant manifolds $\mathcal{M}(Q_0)$ obtained by varying Q_0. Note that, according to (25), each manifold $\mathcal{M}(Q_0)$ is given by

$$r = Q_0 - 5s - z^3 - z.$$

For each manifold, the figure shows the trajectory starting at the initial condition on the manifold with $s_0 = 0$ and $z_0 = -0.1$. It can be checked that, as predicted by the theory, each manifold is invariant for the dynamics of (35). The same figure also shows

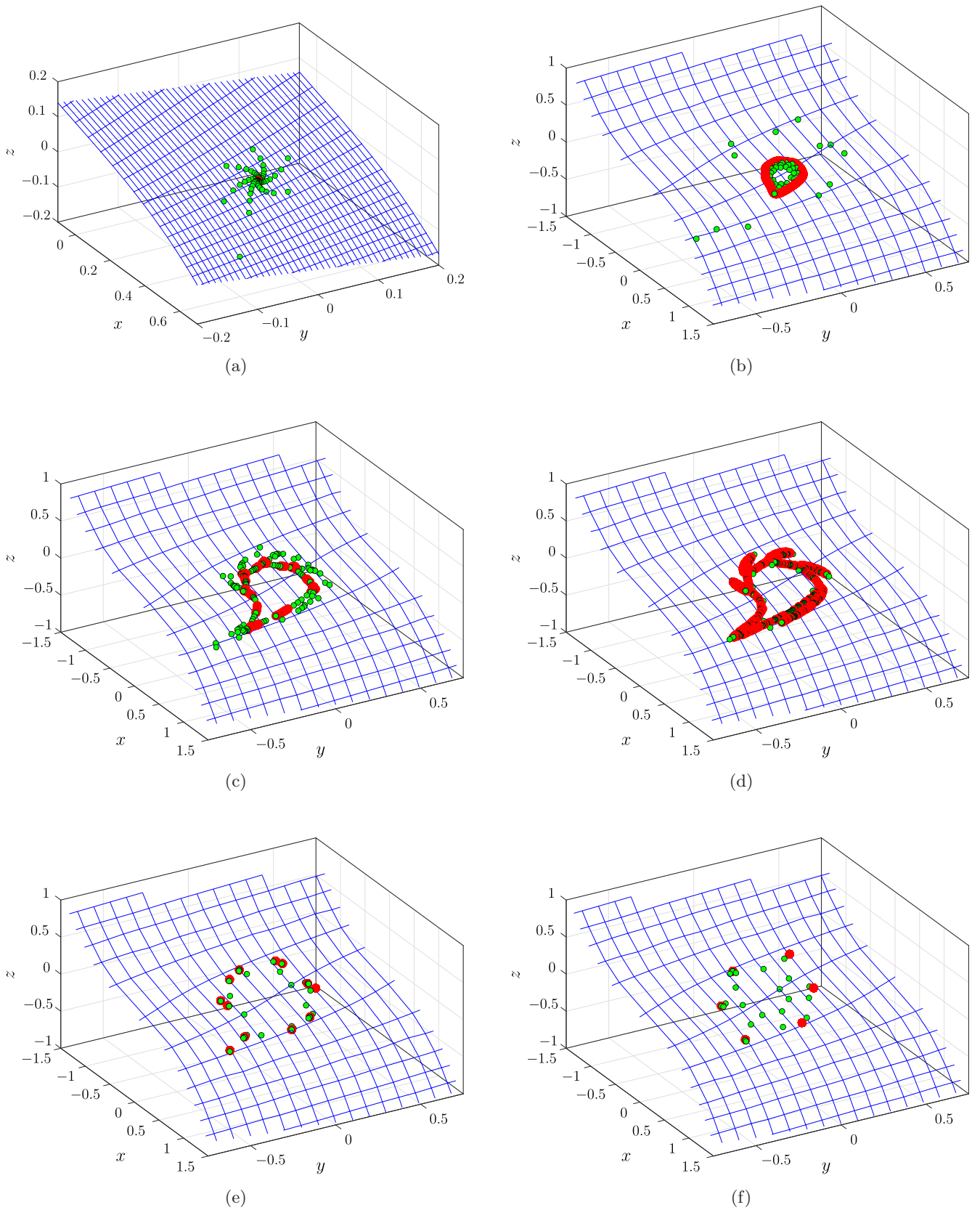

Fig. 18. Different invariant manifolds of the third-order map (35) obtained by varying Q_0. For each manifold, the figure shows the solution starting at $s_0 = 0, z_0 = -0.1$ (green points) and the long-term behavior of the solution (red points): (a) $Q_0 = -0.4$, (b) $Q_0 = -0.3$, (c) $Q_0 = -0.2$, (d) $Q_0 = -0.18$, (e) $Q_0 = -0.1$ and (f) $Q_0 = 0$.

the long-term behavior of the solution and the corresponding attractor. Note that when $Q_0 = -0.4 < -Q_{0,\mathrm{PAH}} = -0.34$, the solution converges to a fixed point. When $Q_0 = -0.3 > -Q_{0,\mathrm{PAH}}$, the solution converges to a closed curve encircling the fixed point. Moreover, when $Q_0 = -0.2$ and $Q_0 = -0.18$, we observe a complex attractor. Finally, when $Q_0 = -0.1$ the attractor appears to be a period-12 cycle, and when $Q_0 = 0$ it is a period-six cycle.

8. Analysis of Memristor Chua's Circuit via DT-FCAM

8.1. *Analysis in the VCD*

Consider the CT MCC in the class $\mathcal{LM}$ shown in Fig. 19. The circuit has an ideal resistor $R > 0$, two ideal capacitors $C_1, C_2 > 0$, an ideal inductor $L > 0$ and an ideal flux-controlled memristor $q_M = \hat{q}_M(\varphi_M)$. The circuit is obtained by replacing the nonlinear resistor in Chua's circuit [Itoh & Chua, 2008] with a memristor.

Let us analyze the corresponding DT MCC circuit in Fig. 20 using DT-FCAM and the new discretization scheme introduced for the memristor. In the VCD, using the CRs of circuit elements, the two KCLs at nodes A and B read as

$$C_1\frac{v_{C1,k+1}-v_{C1,k}}{h} = \frac{v_{C2,k}-v_{C1,k}}{R} - \frac{\hat{q}(\varphi_{M,k+1})-\hat{q}(\varphi_{M,k})}{h}$$

and

$$C_2\frac{v_{C2,k+1}-v_{C2,k}}{h} = i_{L,k} + \frac{v_{C1,k}-v_{C2,k}}{R},$$

respectively, while the two KVLs can be written as

$$L\frac{i_{L,k+1}-i_{L,k}}{h} = -v_{C2,k}$$

and

$$v_{M,k} = v_{C1,k}.$$

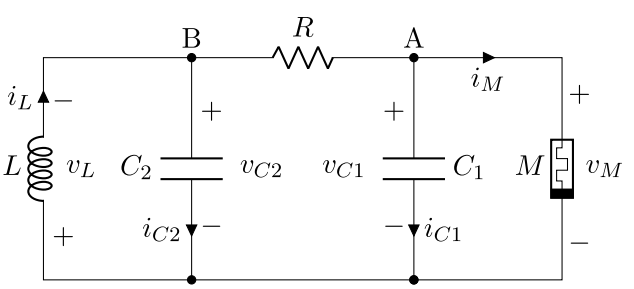

Fig. 19. Continuous-time MCC.

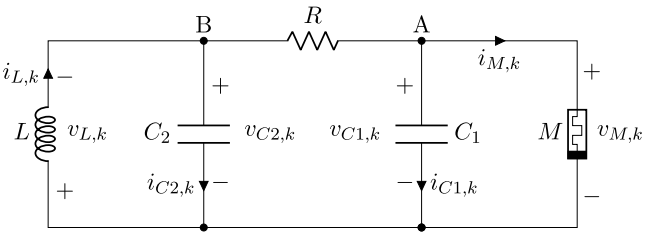

Fig. 20. Discrete-time MCC.

These yield the fourth-order map in the VCD describing the dynamics of MCC,

$$\begin{cases} v_{C1,k+1} = v_{C1,k} - \dfrac{\hat{q}(\varphi_{M,k}+hv_{C1,k})-\hat{q}(\varphi_{M,k})}{C_1} \\ \qquad\qquad + \dfrac{h}{C_1R}(v_{C2,k}-v_{C1,k}), \\ v_{C2,k+1} = v_{C2,k} + \dfrac{h}{C_2}\left[\dfrac{(v_{C1,k}-v_{C2,k})}{R} + i_{L,k}\right], \\ i_{L,k+1} = i_{L,k} - \dfrac{h}{L}v_{C2,k}, \\ \varphi_{M,k+1} = \varphi_{M,k} + hv_{C1,k}. \end{cases} \tag{36}$$

The state variables are $v_{C1,k}, v_{C2,k}, i_{L,k}, \varphi_{M,k}$ and the initial conditions are $v_{C1,0} = v_{C1}(t_0), v_{C2,0} = v_{C2}(t_0), i_{L,0} = i_L(t_0), \varphi_{M,0} = \varphi_M(t_0)$.

8.2. *First integral and invariant manifolds*

From the third equation in (24), we obtain

$$v_{C2,k} = -\frac{L}{h}(i_{L,k+1}-i_{L,k}).$$

Moreover, from the fourth equation, we have

$$v_{C1,k} = \frac{\varphi_{M,k+1}-\varphi_{M,k}}{h}.$$

Substituting in the first equation and rearranging the terms, we have

$$C_1v_{C1,k+1} + \frac{L}{R}i_{L,k+1} + \frac{1}{R}\varphi_{M,k+1} + \hat{q}(\varphi_{M,k+1}) = C_1v_{C1,k} + \frac{L}{R}i_{L,k} + \frac{1}{R}\varphi_{M,k} + \hat{q}(\varphi_{M,k}).$$

Consider the function of the state variables

$$w(v_{C1}, v_{C2}, i_L, \varphi_M) = Cv_{C1} + \frac{Li_L}{R} + \frac{\varphi_M}{R} + \hat{q}(\varphi_M).$$

We have shown that

$$w(v_{C1,k+1}, v_{C2,k+1}, i_{L,k+1}, \varphi_{M,k+1}) = w(v_{C1,k}, v_{C2,k}, i_{L,k}, \varphi_{M,k})$$

along the solutions of (36), i.e. w is a first integral for MCC and it coincides with that of the CT MCC (cf. Corinto and Forti [2017]). Once again, note that this property holds for any step size h.

Now, introduce the subsets of the state space

$$\mathcal{M}(Q_0) = \Big\{(v_{C1}, v_{C2}, i_L, \varphi_M) \in \mathbb{R}^4 : w(v_{C1}, v_{C2}, i_L, \varphi_M) = Cv_{C1} + \frac{Li_L}{R} + \hat{q}(\varphi_M) + \frac{\varphi_M}{R} = Q_0\Big\}, \tag{37}$$

where $Q_0 \in \mathbb{R}$. Each set is a three-dimensional *invariant manifold* for the dynamics of (36) and it is uniquely defined by the *manifold index*

$$Q_0 = Cv_{C1,0} + \frac{Li_{L,0}}{R} + \hat{q}(\varphi_{M,0}) + \frac{\varphi_{M,0}}{R} \tag{38}$$

depending upon the initial conditions for the state variables in the VCD.

8.3. *Analysis in the FCD*

Let us now analyze the MCC of Fig. 21 in the FCD to determine the dynamics on each invariant manifold. Using the CRs of circuit elements, the KCLs at nodes A and B yield

$$C_1\frac{\varphi^0_{C1,k+1} - \varphi^0_{C1,k}}{h} - C_1 v_{C1,0} = \frac{\varphi^0_{C2,k} - \varphi^0_{C1,k}}{R} - \hat{q}(\varphi^0_{M,k} + \varphi_{M,0}) + \hat{q}(\varphi_{M,0})$$

and

$$C_2\frac{\varphi^0_{C2,k+1} - \varphi^0_{C2,k}}{h} - C_2 v_{C2,0} = \frac{\varphi^0_{C1,k} - \varphi^0_{C2,k}}{R} + q^0_{L,k},$$

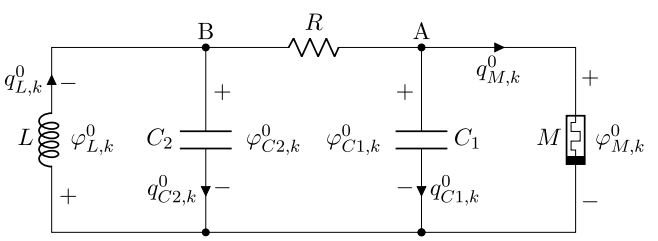

Fig. 21. Discrete-time MCC in the flux–charge domain.

respectively. Moreover, we can write the two KVLs as

$$L\frac{q^0_{L,k+1} - q^0_{L,k}}{h} - Li_{L,0} = -\varphi^0_{C2,k}$$

and

$$\varphi^0_{M,k} = \varphi^0_{C1,k}.$$

Therefore, we obtained the third-order map describing the dynamics of the MRLC circuit in the FCD,

$$\begin{cases} \varphi^0_{C1,k+1} = \varphi^0_{C1,k} + \dfrac{h}{C_1}\left(\dfrac{\varphi^0_{C2,k} - \varphi^0_{C1,k}}{R} - \hat{q}(\varphi^0_{C1,k} + \varphi_{M,0}) + \hat{q}(\varphi_{M,0})\right) + hv_{C1,0}, \\ \varphi^0_{C2,k+1} = \varphi^0_{C2,k} + \dfrac{h}{C_2}\left(\dfrac{\varphi^0_{C1,k} - \varphi^0_{C2,k}}{R} + q^0_{L,k}\right) + hv_{C2,0}, \\ q^0_{L,k+1} = q^0_{L,k} - \dfrac{h}{L}\varphi^0_{C2,k} + hi_{L,0}. \end{cases} \tag{39}$$

The state variables are $\varphi^0_{C1,k}, \varphi^0_{C2,k}, q^0_{L,k}$ and the initial conditions are $\varphi^0_{C1,0} = 0, \varphi^0_{C2,0} = 0, q^0_{L,0} = 0$.

8.4. *Coexisting attractors and bifurcations without parameters*

The change of variables $x_k = \varphi_{M,k}$, $y_k = \varphi^0_{C2,k} - Li_{L,0}$ and $z_k = Rq^0_{L,k} - \varphi_{M,0} - Li_{L,0} + RC_2 v_{C2,0}$ yields from (39) the third-order map

$$\begin{pmatrix} x \\ y \\ z \end{pmatrix} \to \begin{pmatrix} f_1(x,y,z) \\ f_2(x,y,z) \\ f_3(x,y,z) \end{pmatrix} = \begin{pmatrix} x + \dfrac{h}{C_1 R}(y - x - R\hat{q}(x)) + \dfrac{h}{C_1}Q_0 \\ y + \dfrac{h}{C_2 R}(x - y + z) \\ z - \dfrac{hR}{L}y \end{pmatrix}, \tag{40}$$

where Q_0 is given in (38).

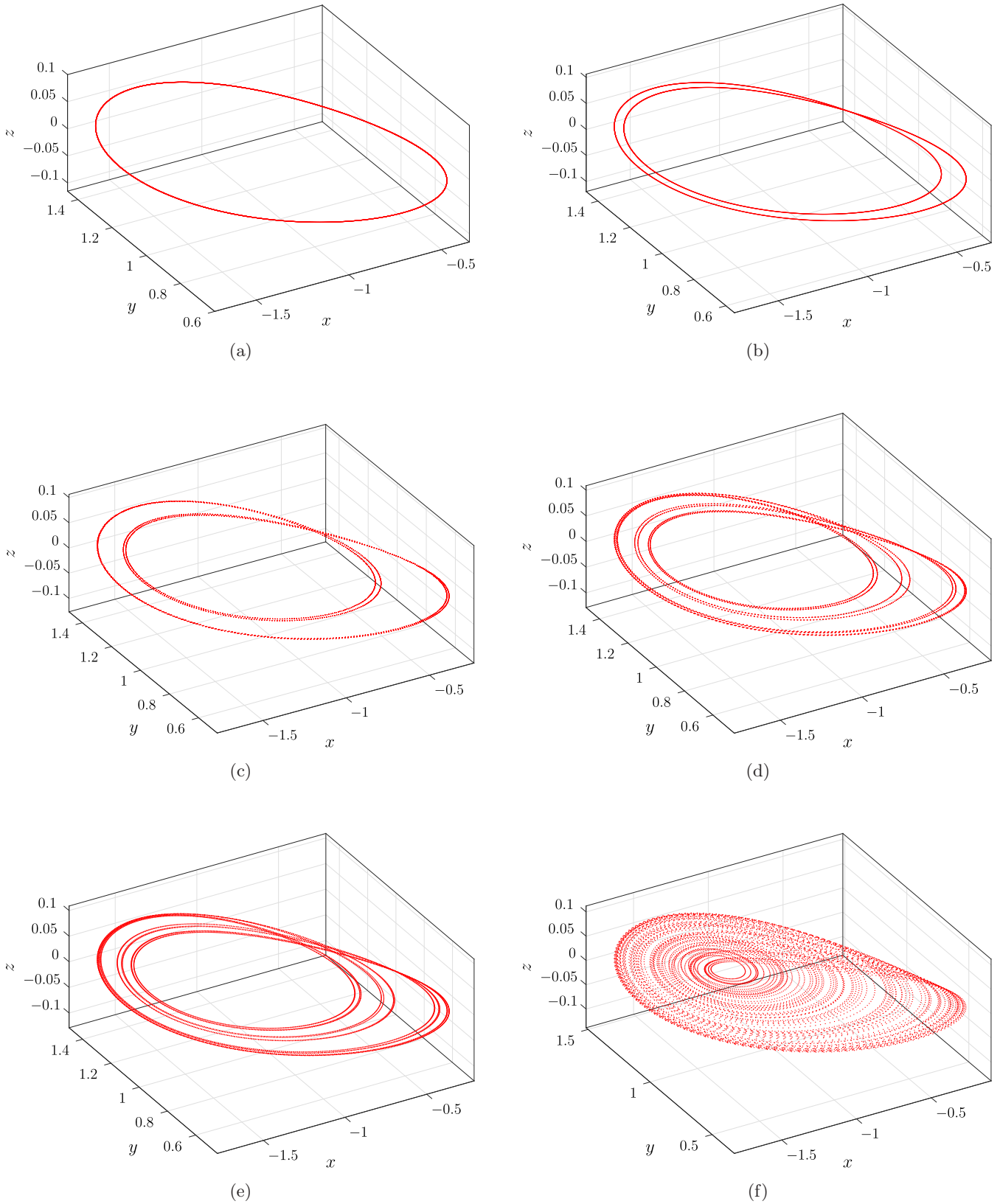

Fig. 22. Long-term behavior of the solutions of the DT MCC (40) when $Q_0 = -0.064$ and for different values of the step size h: (a) $h = 0.0001$, (b) $h = 0.001$, (c) $h = 0.008$, (d) $h = 0.0098$, (e) $h = 0.01$ and (f) $h = 0.02$.

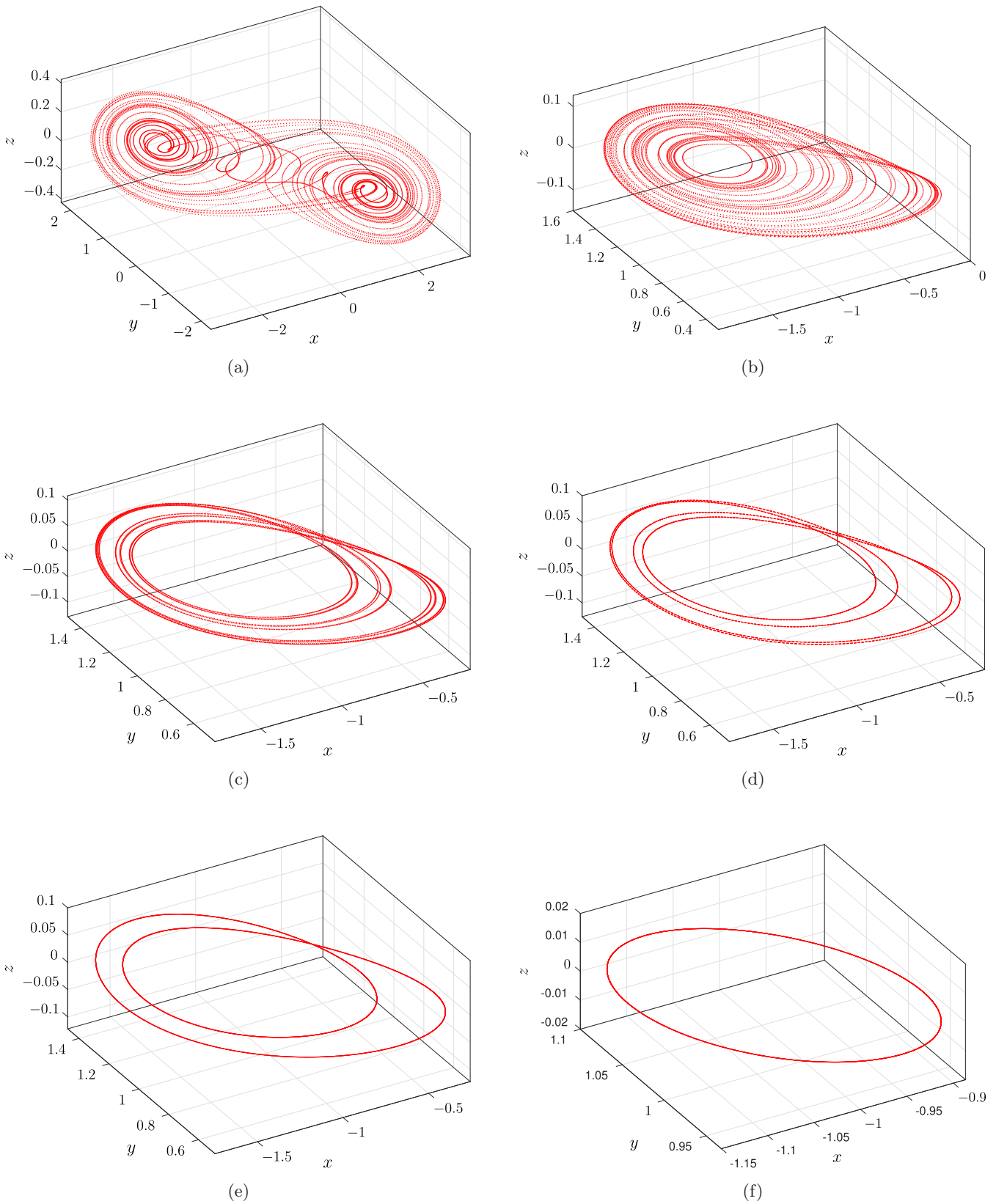

Fig. 23. Long-term behavior of the solutions of (40) when $h = 1.9$ and for different values of the manifold index Q_0: (a) $Q_0 = 0$, (b) $Q_0 = -0.06$, (c) $Q_0 = -0.64$, (d) $Q_0 = -0.645$, (e) $Q_0 = -0.065$ and (f) $Q_0 = -0.078$.

Suppose to choose the normalized circuit parameters $R = 1$, $L = 1/15$, $C_1 = 1/10$ and $C_2 = 1$; moreover, let $\hat{q}(x) = m_0 x + m_1 x^3$, where $m_0 = -8/7$ and $m_1 = 4/63$. For these values and nonlinearity, the corresponding CT Chua's circuit is known to display a complex behavior [Corinto & Forti, 2017]. Next, we want to study through simulations the bifurcations of (40) when the parameter h or Q_0 is varied.

First, consider the bifurcations with respect to h when $Q_0 = -0.064$ is fixed. Figure 22 shows the results obtained from simulations. When $h = 0.0001$, the DT MCC converges to a closed curve. When h is increased, this curve appears to undergo a sequence of bifurcations similar to period-doubling bifurcations. Finally, when $h = 0.02$, we have convergence to a complex single-scroll attractor.

Then, suppose we fix $h = 0.01$ and study the bifurcations with respect to Q_0. Figure 23 shows the results obtained with simulations. When $Q_0 = 0$, MCC displays a complex double-scroll attractor. When $Q_0 = -0.06$, we instead observe a complex single-scroll attractor. By further decreasing Q_0, we observe a sequence of bifurcations similar to inverse period-doubling bifurcations. All these bifurcations are obtained by varying Q_0 through variations of the initial conditions for the state variables in the VCD for fixed circuit parameters, memristor nonlinearity and step size. Along the same line of reasoning as for the MC and MRLC circuits, we conclude that all these different dynamics obtained by varying Q_0 coexist for the DT MCC circuit (36).

9. Conclusion

The paper has introduced a new discretization scheme for a class $\mathcal{LM}$ of nonlinear circuits containing ideal resistors, capacitors, inductors and ideal flux- or charge-controlled memristors. The scheme ensures that the first integrals of CT memristor circuits are preserved exactly in the discretization and that this holds for any step size h. As such, it differs from those typically used in the literature, that typically destroy the first integrals. On this basis, the flux–charge analysis method in Corinto and Forti [2016] has been extended to analyze this class of DT memristor circuits. The method has enabled to rigorously show that the state space of DT memristor circuits in $\mathcal{LM}$ can be foliated in invariant manifolds, which in turn implies the coexistence of infinitely many different attractors (extreme multistability) and the existence of bifurcations without parameters.

One general conclusion of this study is that maps obtained by discretizing via the proposed scheme's memristor circuits in the class $\mathcal{LM}$ are able to display for structural reasons a very rich dynamical behavior. The richness is ascribed to two main properties: First of all, the foliation of the state space in invariant manifolds and the coexistence of infinitely many different dynamics and attractors; second, since the foliation in invariant manifolds holds for any h, this enables to use h as a parameter without destroying the structure of invariant manifolds and, as a consequence, further complexities are obtained by varying h.

We have analyzed in detail a DT MC circuit in $\mathcal{LM}$ showing coexisting dynamics and flip bifurcations due to varying h or the index of the manifold (flip bifurcations without parameters). For the DT MC circuit, there is coexistence of convergent, periodic and complex dynamics. Moreover, for a DT MRLC circuit, we have studied the coexisting convergent and nonconvergent dynamics and Poincaré–Andronov–Hopf bifurcations with or without the parameters. Simulations are also provided to show bifurcations in a higher-order DT memristor Chua's circuit.

We believe the introduced DT maps may be useful to design effective algorithms for applications in the telecommunications field or in the field of random number generators. Investigating these aspects will be the subject of future work on DT memristor circuits.

References

Ascoli, A., Demirkol, A. S., Tetzlaff, R. & Chua, L. O. [2022a] "Edge of chaos theory resolves Smale paradox," *IEEE Trans. Circuits Syst.-I: Regul. Pap.* **69**, 1252–1265.

Ascoli, A., Demirkol, A. S., Tetzlaff, R. & Chua, L. O. [2022b] "Edge of chaos explains Prigogine's instability of the homogeneous," *IEEE J. Emerg. Sel. Top. Circuits Syst.* **12**, 804–820.

Bao, B.-C., Xu, Q., Bao, H. & Chen, M. [2016] "Extreme multistability in a memristive circuit," *Electr. Lett.* **52**, 1008–1010.

Bao, H., Hua, Z., Li, H., Chen, M. & Bao, B. [2021] "Discrete memristor hyperchaotic maps," *IEEE Trans. Circuits Syst.-I: Regul. Pap.* **68**, 4534–4544.

Bao, H., Gu, Y., Xu, Q., Zhang, X. & Bao, B. [2022] "Parallel bi-memristor hyperchaotic map with extreme multistability," *Chaos Solit. Fract.* **160**, 112273.

Buscarino, A., Fortuna, L., Frasca, M. & Gambuzza, L. V. [2013] "A gallery of chaotic oscillators based on HP memristor," *Int. J. Bifurcation and Chaos* **23**, 1330015-1–14.

Chang, H., Li, Y., Yuan, F. & Chen, G. [2019] "Extreme multistability with hidden attractors in a simplest memristor-based circuit," *Int. J. Bifurcation and Chaos* **29**, 1950086-1–17.

Chua, L. O. [1971] "Memristor: The missing circuit element," *IEEE Trans. Circuit Th.* **18**, 507–519.

Corinto, F. & Forti, M. [2016] "Memristor circuits: Flux–charge analysis method," *IEEE Trans. Circuits Syst.-I*: *Regul. Pap.* **63**, 1997–2009.

Corinto, F. & Forti, M. [2017] "Memristor circuits: Bifurcations without parameters," *IEEE Trans. Circuits Syst.-I*: *Regul. Pap.* **64**, 1540–1551.

Corinto, F., Forti, M. & Chua, L. O. [2021] *Nonlinear Circuits and Systems with Memristors*: *Nonlinear Dynamics and Analogue Computing via the Flux–Charge Analysis Method* (Springer, Cham).

Di Marco, M., Forti, M., Pancioni, L., Innocenti, G., Tesi, A. & Corinto, F. [2022] "Oscillatory circuits with a real non-volatile Stanford memristor model," *IEEE Access* **10**, 13650–13662.

Di Marco, M., Forti, M., Pancioni, L. & Tesi, A. [2023] "Convergence of discrete-time cellular neural networks with application to image processing," *Int. J. Bifurcation and Chaos* **33**, 2350115-1–25.

Escudero, M., Spiga, S., Di Marco, M., Forti, M., Innocenti, G., Tesi, A., Corinto, F. & Brivio, S. [2023] "Chua's circuit with tunable nonlinearity based on a nonvolatile memristor: Design and realization," *IEEE Trans. Circuits Syst.-I*: *Regul. Pap.*, doi: 10.1109/TCSI.2023.3323854.

Hale, J. & Koçak, H. [1991] *Dynamics and Bifurcations*, Texts in Applied Mathematics (Springer-Verlag, NY).

Hens, C., Banerjee, R., Feudel, U. & Dana, S. [2012] "How to obtain extreme multistability in coupled dynamical systems," *Phys. Rev. E* **85**, 035202(R).

Huang, T., Chen, Y., Zeng, Z. & Chua, L. [2021] "Editorial Special Issue for 50th birthday of memristor theory and application of neuromorphic computing based on memristor: Part I," *IEEE Trans. Circuits Syst.-I*: *Regul. Pap.* **68**, 4417–4418.

Ishaq Ahamed, A. & Lakshmanan, M. [2013] "Nonsmooth bifurcations, transient hyperchaos and hyperchaotic beats in a memristive Murali–Lakshmanan–Chua circuit," *Int. J. Bifurcation and Chaos* **23**, 1350098-1–28.

Itoh, M. & Chua, L. O. [2008] "Memristor oscillators," *Int. J. Bifurcation and Chaos* **18**, 3183–3206.

Itoh, M. & Chua, L. O. [2014] "Memristor cellular automata and memristor discrete-time cellular neural networks," in *Memristor Networks* (Springer, Cham), pp. 649–713, doi: 10.1007/978-3-319-02630-5_30.

James, A. P., Salama, K. N., Li, H., Biolek, D., Indiveri, G. & Chua, L. O. [2018] "Guest Editorial: Special Issue on large-scale memristive systems and neurochips for computational intelligence," *IEEE Trans. Emerg. Top. Comput. Intell.* **2**, 320–323.

Kumar, S., Strachan, J. P. & Williams, R. S. [2017] "Chaotic dynamics in nanoscale NbO_2 Mott memristors for analogue computing," *Nature* **548**, 318–321.

Kuznetsov, Y. A. [1998] *Elements of Applied Bifurcation Theory*, Applied Mathematical Sciences, Vol. 112 (Springer, NY).

Li, H., Hua, Z., Bao, H., Zhu, L., Chen, M. & Bao, B. [2020] "Two-dimensional memristive hyperchaotic maps and application in secure communication," *IEEE Trans. Ind. Electron.* **68**, 9931–9940.

Liang, Y., Wang, G., Chen, G., Dong, Y., Yu, D. & Iu, H. H.-C. [2020] "S-type locally active memristor-based periodic and chaotic oscillators," *IEEE Trans. Circuits Syst.-I*: *Regul. Pap.* **67**, 5139–5152.

Sebastian, A., Le Gallo, M., Burr, G. W., Kim, S., BrightSky, M. & Eleftheriou, E. [2018] "Tutorial: Brain-inspired computing using phase-change memory devices," *J. Appl. Phys.* **124**, 111101.

Sirakoulis, G. C., Ascoli, A., Tetzlaff, R. & Yu, S. [2022] "Guest Editorial memristive circuits and systems for edge-computing applications," *IEEE J. Emerg. Sel. Top. Circuits Syst.* **12**, 717–722.

Solan, E. & Ochs, K. [2018] "Wave digital emulation of general memristors," *Int. J. Circuit Theory Appl.* **46**, 2011–2027.

Strukov, D. B., Snider, G. S., Stewart, D. R. & Williams, R. S. [2008] "The missing memristor found," *Nature* **453**, 80–83.

Williams, R. S. [2017] "What's next? [The end of Moore's law]," *Comput. Sci. Eng.* **19**, 7–13.

Yang, J. J. & Williams, R. S. [2013] "Memristive devices in computing system: Promises and challenges," *ACM J. Emerg. Technol. Comput. Syst.* **9**, 11-1–20.

Appendix A

Consider the second-order map (28). We wish to apply the procedure in Hale and Koçak [1991, Sec. 15.5] to evaluate the coefficient a when $Q_0 = 0$, in which case the map has a unique fixed point $(\overline{x}, \overline{y}) = (0, 0)$, and moreover, from (32), we have

$h_{\mathrm{PAH}} = RC$. The Jacobian of the map at $(0,0)$, evaluated at $h = h_{\mathrm{PAH}}$, is given by

$$J = \begin{pmatrix} 1 & \dfrac{h_{\mathrm{PAH}}}{C} \\ -\dfrac{h_{\mathrm{PAH}}}{L} & 1 - \dfrac{h_{\mathrm{PAH}} R}{L} \end{pmatrix} = \begin{pmatrix} 1 & R \\ -\dfrac{RC}{L} & 1 - \dfrac{R^2 C}{L} \end{pmatrix},$$

and it has the complex eigenvalues

$$\lambda_{1,2} = \alpha \pm j\beta = -\frac{CR^2 - 2L}{2L} \pm j\frac{R\sqrt{4CL - C^2R^2}}{2L}$$

provided $R < 2\sqrt{L/C}$. The change of variables

$$\begin{pmatrix} S \\ T \end{pmatrix} = \begin{pmatrix} -\dfrac{R}{2} & \dfrac{\sqrt{4CL - C^2R^2}}{2C} \\ 1 & 1 \end{pmatrix} \begin{pmatrix} x \\ y \end{pmatrix}$$

yields the following map: $(S,T) \to (G_1(S,T), G_2(S,T))$, where the linear part is in normal Jordan form,

$$\begin{pmatrix} G_1(S,T) \\ G_2(S,T) \end{pmatrix} = \begin{pmatrix} -\dfrac{CR^2 - 2L}{2L} & -\dfrac{R\sqrt{4CL - C^2R^2}}{2L} \\ \dfrac{R\sqrt{4CL - C^2R^2}}{2L} & -\dfrac{CR^2 - 2L}{2L} \end{pmatrix} \begin{pmatrix} S \\ T \end{pmatrix} + \begin{pmatrix} 0 \\ -\dfrac{R(T\sqrt{4CL - C^2R^2} - CRS)^3}{4C^2\sqrt{4CL - C^2R^2}} \end{pmatrix}. \quad \text{(A.1)}$$

Now, we are in a position to use Hale and Koçak [1991, Eq. (15.25)] to evaluate the coefficient a, which is a function of the second- and third-order derivatives of the nonlinear terms of map (A.1) and the eigenvalues of J. After some tedious yet quite straightforward computations and manipulations, it is possible to show that we have

$$a(Q_0 = 0) = \frac{3R}{16}\left(2\frac{L}{C} - R^2 - R\right).$$